EUROPEAN ORGANIZATION FOR NUCLEAR RESEARCH

Event-shape engineering for the D-meson elliptic flow in mid-central Pb–Pb collisions at $\sqrt{s_{\mathrm{NN}}} = 5.02$ TeV

ALICE Collaboration[*]

Abstract

The production yield of prompt D mesons and their elliptic flow coefficient v_2 were measured with the Event-Shape Engineering (ESE) technique applied to mid-central (10–30% and 30–50% centrality classes) Pb–Pb collisions at the centre-of-mass energy per nucleon pair $\sqrt{s_{\mathrm{NN}}} = 5.02$ TeV, with the ALICE detector at the LHC. The ESE technique allows the classification of events, belonging to the same centrality, according to the azimuthal anisotropy of soft particle production in the collision. The reported measurements give the opportunity to investigate the dynamics of charm quarks in the Quark–Gluon Plasma and provide information on their participation in the collective expansion of the medium. D mesons were reconstructed via their hadronic decays at mid-rapidity, $|\eta| < 0.8$, in the transverse momentum interval $1 < p_{\mathrm{T}} < 24$ GeV/c. The v_2 coefficient is found to be sensitive to the event-shape selection confirming a correlation between the D-meson azimuthal anisotropy and the collective expansion of the bulk matter, while the per-event D-meson yields do not show any significant modification within the current uncertainties.

[*]See Appendix A for the list of collaboration members

1 Introduction

Quantum Chromo-Dynamics (QCD) calculations on the lattice predict the existence of a plasma of deconfined quarks and gluons, known as the Quark–Gluon Plasma (QGP) [1–4]. The transition from the hadronic phase to the QGP state occurs at high temperatures and energy densities, which can be reached in collisions of heavy nuclei at ultra-relativistic energies. The QGP created in ultra-relativistic heavy-ion collisions was found to behave as a nearly ideal fluid (i.e. with a small shear viscosity over entropy density ratio, η/s), undergoing an expansion that can be described by relativistic hydrodynamics [5–10].

Heavy flavours (charm and beauty quarks), due to their large masses, $m_c \approx 1.3$ GeV/c^2 and $m_b \approx 4.5$ GeV/c^2, are predominantly produced in hard-scattering processes characterised by timescales shorter than the QGP formation time [11–14]. Thus, they experience the entire evolution of the medium interacting with its constituents via inelastic (gluon radiation) [15–17] and elastic (collisional) [18] QCD processes. Such interactions with the medium constituents can also lead to a modification of the hadronisation mechanism with respect to the fragmentation in vacuum: a significant fraction of low- and intermediate-momentum charm and beauty quarks can hadronise via recombination with other quarks from the medium [19–21].

Heavy-flavour hadrons are effective probes of the properties of the medium produced in heavy-ion collisions. A strong modification of their transverse-momentum (p_{T}) distributions in heavy-ion collisions with respect to pp collisions was observed at RHIC [22–25] and LHC energies [26–32]. In particular, the observed suppression of the yield of heavy-flavour hadrons in central nucleus–nucleus collisions relative to pp collisions scaled by the number of nucleon–nucleon collisions provides compelling evidence of the heavy-quark energy loss in deconfined strongly-interacting matter [13, 17].

Further insight into the interactions of heavy quarks with the medium can be obtained through measurements of the azimuthal distributions of heavy-flavour hadrons in heavy-ion collisions. The initial spatial anisotropy present in the early stages of nucleus–nucleus collisions is converted via multiple interactions into an azimuthally anisotropic distribution in momentum space of the produced particles [33, 34]. This anisotropy can be characterised in terms of the Fourier coefficients v_n of the azimuthal distribution of particle momenta relative to the symmetry-plane angles Ψ_n (for the nth harmonic) [34, 35]. The values of the Fourier coefficients depend on the geometry of the collision, the fluctuations in the distributions of nucleons within the nuclei [36], and the dynamics of the expansion. The second-order coefficient $v_2 = \langle \cos[2(\varphi - \Psi_2)]\rangle$, where φ is the particle momentum azimuthal angle and the brackets indicate the average over all the measured particles in the considered events, is usually denoted as elliptic flow. In non-central heavy-ion collisions, it represents the dominant term in the Fourier expansion [33, 35]. The measurement of the azimuthal anisotropy of heavy-flavour hadrons at low p_{T} is sensitive to whether charm quarks take part in the collective expansion of the medium [37], as well as to the fraction of heavy-flavour hadrons hadronising via recombination with flowing light quarks [38, 39]. At high p_{T}, it can constrain the path-length dependence of heavy-quark in-medium energy loss [40, 41]. A positive v_2 in the heavy-flavour sector was observed at RHIC in Au–Au collisions at a centre-of-mass energy per nucleon pair $\sqrt{s_{\mathrm{NN}}} = 200$ GeV [22, 42, 43] and at the LHC in Pb–Pb collisions at $\sqrt{s_{\mathrm{NN}}} = 2.76$ TeV [44–47]. Evidence of a positive D-meson v_2 was also reported in Pb–Pb collisions at $\sqrt{s_{\mathrm{NN}}} = 5.02$ TeV by the ALICE [48] and CMS [49] Collaborations. The anisotropic flow of beauty quarks was investigated by the CMS Collaboration through the measurement of non-prompt J/ψ elliptic flow [30]. The D-meson results are described by theoretical calculations including mechanisms that impart a positive v_2 to charm quarks through the interactions with the hydrodynamically-expanding medium, namely collisional processes, and recombination of charm and light quarks [50–59]. According to these model calculations, the same mechanisms affect the beauty-quark propagation in the medium, although the beauty-hadron v_2 is expected to be smaller than that of charm hadrons and to have a different transverse momentum dependence due to the large mass of the b quarks. Precise measurements of v_2 of heavy-flavour hadrons help to constrain model parameters, e.g., the heavy-quark spatial diffusion coefficient D_s in the QGP,

2

which is related to the relaxation time (or the time scale for equilibration) of the heavy quarks inside the QGP [48, 60].

The Event Shape Engineering (ESE) technique [61] can be used to further investigate the dynamics of heavy quarks in the medium. This technique has already been exploited in the light-flavour sector to study the interplay between the initial geometry of the nucleus–nucleus collisions and the subsequent evolution of the system [62, 63], and to investigate the Chiral Magnetic Effect (CME) [64, 65]. The ESE technique is based on the observation of a large event-by-event v_n variation at fixed collision centrality [66]. Hydrodynamic calculations show a linear correlation between the final state v_2 (and v_3) and the corresponding eccentricities in the initial state ε_2 (and ε_3) for small values of η/s [67–69]. These observations suggest the possibility to select heavy-ion collisions with different initial geometrical shape on the basis of the magnitude of the average bulk flow.

The ESE technique provides a tool to investigate the correlation between the flow coefficients of D mesons and soft hadrons: measuring the D-meson v_2 in classes of events in a given centrality interval, but with different magnitude of the average event flow can be useful to study the interplay between the anisotropic flow of heavy quarks and that of the bulk matter. In addition, it could provide insights on how the fluctuations in the initial geometry of the system affect the path-length-dependent energy loss experienced by the heavy quarks in the QGP. For these reasons, the application of the ESE technique to the D-meson v_2 measurements could be exploited to infer more information on the dynamics of the charm quark in the QGP and has the potential to set additional constraints on parameters of model calculations implementing heavy-quark transport in an hydrodynamically expanding medium [70]. Model calculations for the correlation between the v_2 values of soft hadrons and heavy-flavour mesons on an event-by-event basis have recently become available. A linear correlation between the high-p_T D-meson v_2, which originates from the path-length dependence of in-medium energy loss, and the elliptic flow of charged hadrons is predicted in [71], based on a model for charm-quark energy loss in a medium described event-by-event with viscous hydrodynamics. Within the heavy-quark transport model of [72], an almost linear correlation is obtained between the v_2 of pions and that of D^0 mesons with $p_T > 2$ GeV/c, which is dominated by low-p_T mesons and is therefore sensitive to the degree of thermalisation of charm quarks with the collectively expanding medium. According to these calculations, the initial system ellipticity is converted into parton flow with a similar efficiency for bulk and charm quarks, despite the different production mechanisms, dynamics and hadronisation of heavy quarks and light partons forming the bulk of the medium.

Finally, the measurement of the D-meson yields at low and intermediate p_T in ESE-selected events allows the investigation of a possible interplay between elliptic and radial flow, already observed for charged and identified particles [62]. This observation is possibly related to the correlation between the density of participant nucleons and the initial eccentricity of the collision. For high-p_T D mesons, the measurement of the yields in collisions with different initial eccentricity via the ESE technique could further constrain in-medium energy loss models.

In this paper, the D^0, D^+ and D^{*+} meson v_2 in Pb–Pb collisions at $\sqrt{s_{\mathrm{NN}}} = 5.02$ TeV in the 10–30% centrality class are presented and compared to the results in the 30–50% centrality class published in [48]. The D^0 and D^+ v_2 obtained with ESE and the measurement of D-meson yield ratios in ESE-selected events in the 10–30% and 30–50% centrality classes are reported as well.

2 Data analysis

The D^0, D^+ and D^{*+} mesons were reconstructed at mid-rapidity, exploiting the tracking and particle identification capabilities of the ALICE detector at the LHC. A detailed description of the ALICE experimental apparatus and its performance can be found in [73, 74]. The main detectors used for the analysis presented in this paper are the Inner Tracking System (ITS), a six-layer silicon detector

used to track charged particles and for the reconstruction of primary and secondary vertices; the Time Projection Chamber (TPC), which provides track reconstruction as well as particle identification via the measurement of the specific ionisation energy loss dE/dx; the Time-Of-Flight (TOF) detector, an array of Multi-Gap Resistive Plate Chambers that provides particle identification via the measurement of the flight time of the particles. These detectors cover the pseudorapidity interval $|\eta| < 0.9$ and are located in a large solenoidal magnet providing a uniform magnetic field of 0.5 T parallel to the LHC beam direction. In addition, two detectors were used for the event selection and classification: the V0 detector, which consists of two arrays of 32 scintillators each, covering the full azimuth in the pseudorapidity intervals $-3.7 < \eta < -1.7$ (V0C) and $2.8 < \eta < 5.1$ (V0A); and the Zero Degree Calorimeters (ZDC), located at 112.5 m from the interaction point on either side, to detect spectator neutrons and protons of the colliding nuclei.

The analysed data sample consists of Pb–Pb collisions at $\sqrt{s_{\mathrm{NN}}} = 5.02$ TeV collected using a minimum-bias interaction trigger that required coincident signals in both scintillator arrays of the V0 detector. Events were selected offline by using the V0 and the neutron ZDC timing information, to remove contaminations produced by the interaction of the beams with residual gas in the vacuum pipe. Only events with a reconstructed primary vertex within ± 10 cm from the centre of the detector along the beam line were analysed. Events satisfying the aforementioned selections were divided in centrality classes, defined in terms of percentiles of the hadronic Pb–Pb cross section. This classification was based on a fit to the sum of the signal amplitudes measured in the V0 detectors. The fit function assumes the Glauber model [75, 76] combined with a two-component model for particle production [77]. The number of events in each centrality class considered for this analysis (10–30% and 30–50%) is about 20.7×10^6, corresponding to an integrated luminosity of about 13 μb^{-1}. The events in each centrality class were further divided in samples with different average elliptic anisotropy of final-state particles, selected according to the magnitude of the second-order harmonic reduced flow vector q_2 [69,78], defined as

$$q_2 = |\boldsymbol{Q}_2|/\sqrt{M}, \tag{1}$$

where M is the multiplicity (number of tracks used in the q_2 calculation) and

$$\boldsymbol{Q}_2 = \left(\begin{array}{c} \sum_{i=1}^{M} \cos(2\varphi_i) \\ \sum_{i=1}^{M} \sin(2\varphi_i) \end{array} \right) \tag{2}$$

is the second-order flow vector, which is built starting from the azimuthal angles (φ_i) of the considered particles. The denominator in Eq. 1 is introduced to remove the dependence of $|\boldsymbol{Q}_2|$ on $\sqrt{M}$ in the absence of flow [69].

The $\boldsymbol{Q}_2$ vector was measured using charged tracks reconstructed in the TPC (q_2^{TPC}), with $|\eta| < 0.8$ and $0.2 < p_{\mathrm{T}} < 5$ GeV/c, to exploit the good φ resolution of the TPC and the large multiplicity at midrapidity, which are crucial to maximise the selectivity of q_2. In order to remove autocorrelations between D mesons and q_2, the tracks used to form the D-meson candidates were excluded from the computation of q_2. However, with this definition of q_2, some residual non-flow correlations (i.e. correlations among particle emission angles not induced by the collective expansion but rather by particle decays and jet production) could still be included. As shown in [62], the introduction of a pseudorapidity separation of more than one unit between the region used to calculate q_2 and the region used to measure the observables would suppress unwanted non-flow contributions. Therefore, to investigate a possible effect induced by non-flow contaminations, q_2 was also measured using the V0A detector (q_2^{V0A}), allowing for a pseudorapidity separation of at least 2 units between the D-meson decay tracks and the particles used for the q_2 determination. In this case, the $\boldsymbol{Q}_2$ vector was calculated from the azimuthal distribution of the energy deposition measured in the V0A detector, and its components are given by

$$Q_{2,x} = \sum_{i=1}^{N_{\mathrm{sectors}}} w_i \cos(2\varphi_i), \quad Q_{2,y} = \sum_{i=1}^{N_{\mathrm{sectors}}} w_i \sin(2\varphi_i), \tag{3}$$
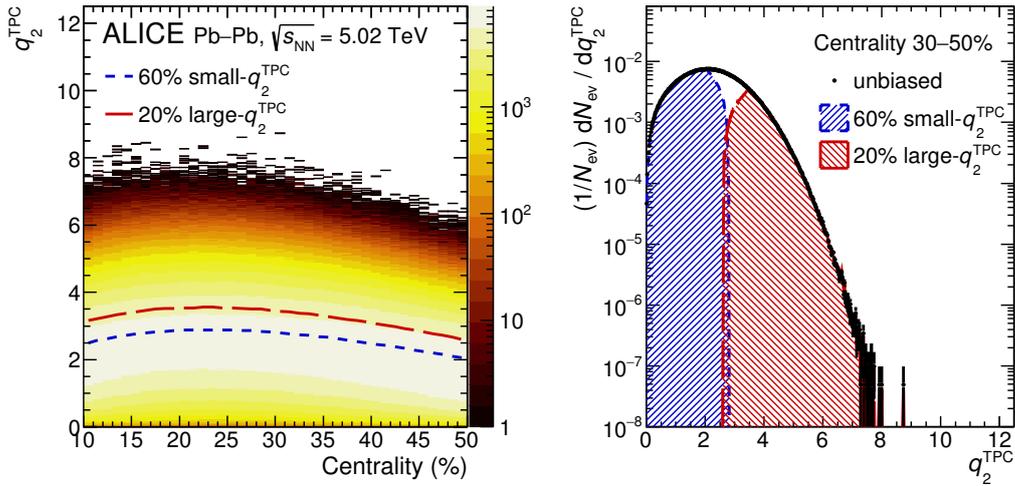
Figure 1: Left: distribution of q_2^{TPC} (see text for details) as a function of centrality in Pb–Pb collisions at $\sqrt{s_{NN}} = 5.02$ TeV. The red long-dashed and the blue short-dashed lines represent the limits for the 20% and the 60% of events with largest and smallest q_2^{TPC}, respectively. Right: q_2^{TPC} distributions for the unbiased, small-q_2^{TPC} and large-q_2^{TPC} samples for the 30–50% centrality class (see text for details).

where the sum runs over the 32 sectors ($N_{sectors}$) of the V0A detector, φ_i is the angle of the centre of the sector i and w_i is the amplitude measured in sector i, once the gain equalisation method [79] is applied to correct effects of non-uniform acceptance. The comparison between the two ESE selections is discussed in Sec. 2.1.

The left panel of Fig. 1 shows the centrality dependence of the q_2^{TPC} distribution. As expected in case of large initial-state fluctuations, the q_2 distribution is broad and reaches values larger than twice the mean value [61]. Moreover, because of the different average elliptic flow and multiplicity, the q_2 distribution changes as a function of centrality. Hence, a selection on a fixed value of q_2 would induce a non-flat centrality distribution, that would spoil the event-shape selection. For this reason, the selection of the events according to their q_2 was performed by defining q_2 percentiles in 1%-wide centrality intervals. The results presented in the following sections are obtained in two ESE-selected classes, corresponding to the 60% and the 20% of events with smallest and largest q_2, respectively. The q_2^{TPC} distributions for these classes in the 30–50% centrality interval are displayed in the right panel of Fig. 1. In the following, we will refer to these two classes as "small-q_2" and "large-q_2". In case of no event-shape selection, we will use the "unbiased" term.

The D mesons, together with their charge conjugates, were reconstructed via their hadronic decay channels $D^0 \rightarrow K^-\pi^+$, $D^+ \rightarrow K^-\pi^+\pi^+$ and $D^{*+} \rightarrow D^0\pi^+ \rightarrow K^-\pi^+\pi^+$. The D-meson candidates were built combining pairs and triplets of tracks with proper charge sign, $|\eta| < 0.8$, $p_T > 0.4$ GeV/c, a minimum number of 70 (out of 159) associated space points in the TPC and no less than two hits (out of six) in the ITS, with at least one in the two innermost layers. For the soft pion produced in the D^{*+} decay, also tracks reconstructed only in the ITS, with at least three associated hits and with $p_T > 0.1$ GeV/c, were considered. These selections limit the D-meson rapidity acceptance, which drops steeply to zero for $|y| > 0.6$ for $p_T = 1$ GeV/c and $|y| > 0.8$ for $p_T > 5$ GeV/c. Therefore, a p_T-dependent fiducial acceptance selection, $|y_D| < y_{fid}(p_T)$, was applied. The selection value, $y_{fid}(p_T)$, was defined according to a second-order polynomial function, increasing from 0.6 to 0.8 in the range $1 < p_T < 5$ GeV/c, and fixed to a constant value of 0.8 for $p_T > 5$ GeV/c.

The D-meson candidate selection strategy for the reduction of the combinatorial background is similar to the one used in previous analyses [45, 48]. The selection of the D^0 and D^+ decay topology was based

5

Centrality class	Detector for ψ_2	Event-shape class	Event-plane resolution R_2
10–30%	V0	unbiased	0.8223 ± 0.0001
		small-q_2^{TPC}	0.7809 ± 0.0001
		large-q_2^{TPC}	0.9058 ± 0.0001
	V0C	unbiased	0.7669 ± 0.0001
		small-q_2^{V0A}	0.7390 ± 0.0001
		large-q_2^{V0A}	0.8223 ± 0.0001
30–50%	V0	unbiased	0.7708 ± 0.0001
		small-q_2^{TPC}	0.7301 ± 0.0001
		large-q_2^{TPC}	0.8646 ± 0.0001
	V0C	unbiased	0.7077 ± 0.0001
		small-q_2^{V0A}	0.6822 ± 0.0001
		large-q_2^{V0A}	0.7597 ± 0.0001

Table 1: Event-plane resolution R_2 in the 10–30% and 30–50% centrality classes for the unbiased, small-q_2 and large-q_2 samples. The quoted uncertainty is statistical only.

on the reconstruction of secondary vertices with a separation of a few hundred microns from the primary vertex ($c\tau \simeq 123$ and 312 μm for D^0 and D^+, respectively [80]). The main variables used to enhance the statistical significance and the signal-to-background ratio are the displacement of the decay tracks from the interaction vertex, the separation between the secondary and primary vertices and the pointing angle of the reconstructed D-meson momentum to the primary vertex. In the case of the strong decay of the D^{*+} meson, the secondary vertex cannot be resolved from the primary vertex, and therefore geometrical selections were applied on the displaced decay-vertex topology of the produced D^0 mesons. In addition, for D^0 and D^+ mesons, the normalised difference between the measured and expected transverse-plane impact parameters of each of the decay particles and the transverse-plane impact parameter to the primary vertex (d_0^{xy}) of the D^+-meson candidates were applied to suppress the fraction of D mesons coming from beauty-hadron decays (denoted by "feed-down" in the following) and hence reduce the associated systematic uncertainty. These selections were found to be especially effective for D^+ mesons, for which a rejection of the feed-down contribution up to 50% at high p_T was achieved. The selection criteria for each D-meson species were optimised as a function of p_T independently for the two centrality classes, because of the different combinatorial background. Within a given centrality class, the same selection criteria were applied in the different ESE-selected samples. In order to further reduce the combinatorial background, a particle identification for charged pions and kaons with the TPC and TOF detectors was applied, using a selection in units of resolution (at ± 3 σ) around the expected mean values of $\mathrm{d}E/\mathrm{d}x$ and time of flight, respectively.

Monte Carlo simulations with a detailed description of the detector and its response, based on the GEANT3 transport package [81], were used to study the signal invariant-mass distributions and the reconstruction efficiencies, as described in the following. In the Monte Carlo simulation, the underlying Pb–Pb events at $\sqrt{s_{NN}} = 5.02$ TeV were simulated using the HIJING v1.383 generator [82] and $c\bar{c}$ or $b\bar{b}$ pairs were added with the PYTHIA v6.421 generator [83] with Perugia-2011 tune [84]. The generated D mesons were forced to decay into the hadronic channels of interest for the analysis.

The D-meson elliptic flow, v_2, is measured using the Event-Plane (EP) method [35]. This analysis technique relies on the event-by-event estimate of the second-order harmonic symmetry plane Ψ_2 using the so-called event-plane angle

$$\psi_2 = \frac{1}{2} \tan^{-1} \left(\frac{Q_{2,y}}{Q_{2,x}} \right). \tag{4}$$

For the measurements of v_2 in the unbiased and q_2^{TPC}-selected samples, $\boldsymbol{Q}_2$ was estimated with the full
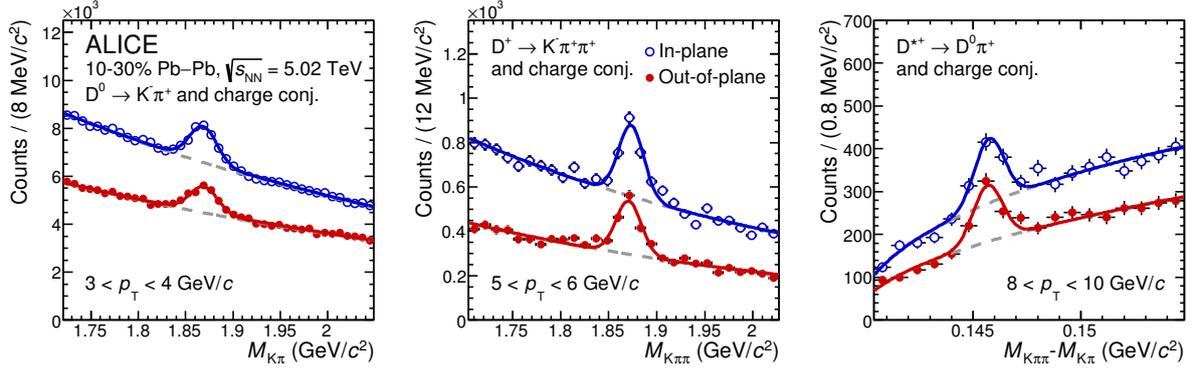
Figure 2: Invariant-mass distributions of D^0 candidates (left panel), D^+ candidates (middle panel) and mass-difference for D^{*+} candidates (right panel) in three p_T intervals for the two $\Delta\varphi$ regions used in the EP method for Pb–Pb collisions in the 10–30% centrality class at $\sqrt{s_{NN}} = 5.02$ TeV. The solid curves represent the total fit functions and the dotted curves the background functions, as described in the text.

V0 detector using Eq. 3 (with $N_{sectors}$ corresponding to the 64 sectors of the full V0 detector). In case of the ESE selection based on q_2^{V0A}, only the 32 sectors of the V0C were used for the ψ_2 determination, to avoid autocorrelations with the q_2 measurement.

After the topological and kinematical selections, the D-meson candidates were divided in two samples, according to their azimuthal angle relative to the event-plane angle $\Delta\varphi = \varphi_D - \psi_2$, namely in-plane ($]-\frac{\pi}{4}, \frac{\pi}{4}]$ and $]\frac{3\pi}{4}, \frac{5\pi}{4}]$) and out-of-plane ($]\frac{\pi}{4}, \frac{3\pi}{4}]$ and $]\frac{5\pi}{4}, \frac{7\pi}{4}]$). The separation of at least 0.9 units of pseudorapidity ($|\Delta\eta| > 0.9$) between the D mesons and the particles used to measure ψ_2, naturally ensured by the selection of D-meson decay tracks and the V0 (V0C) acceptance, suppresses non-flow contributions. The v_2 can therefore be expressed by the following equation [45]

$$v_2\{EP\} = \frac{1}{R_2} \frac{\pi}{4} \frac{N_{\text{in-plane}} - N_{\text{out-of-plane}}}{N_{\text{in-plane}} + N_{\text{out-of-plane}}}, \tag{5}$$

where $N_{\text{in-plane}}$ and $N_{\text{out-of-plane}}$ are the D-meson raw yields in the two $\Delta\varphi$ intervals. The raw yields can be directly used in Eq. 5, without an efficiency correction, since simulations showed that the D-meson reconstruction and selection efficiencies do not depend on $\Delta\varphi$ [45]. The factor $1/R_2$ in Eq. 5 is the correction due to the finite resolution of the estimated ψ_2 angle. In case of v_2 measurements in the unbiased and q_2^{TPC}-selected samples, the event-plane resolution R_2 was determined by correlating three sub-events of charged particles reconstructed in the V0 itself, in the positive ($0 < \eta < 0.8$) and negative ($-0.8 < \eta < 0$) semivolumes of the TPC [35]. In case of ESE selection based on q_2^{V0A}, the three sub-events considered were the charged particles reconstructed in the V0C, in the V0A, and in the full volume of the TPC ($|\eta| < 0.8$). The values of R_2 estimated in the 10–30% and 30–50% centrality classes, for the unbiased, small-q_2 and large-q_2 samples are reported in Tab. 1. The R_2 factor is higher (lower) in the large-q_2 (small-q_2) class with respect to that evaluated for the unbiased sample and similarly in the V0 case than in the V0C one, since the event-plane resolution R_2 increases with increasing $v_2\sqrt{M}$ [35].

The in-plane and out-of-plane raw yields were obtained by fitting the invariant-mass distributions $M(K\pi)$ for D^0 candidates, $M(K\pi\pi)$ for D^+ candidates and the mass-difference $\Delta M = M(K\pi\pi) - M(K\pi)$ distributions for D^{*+} candidates in each centrality class. The fit function was composed by a Gaussian distribution to describe the signal and an exponential term for the background of D^0 and D^+ candidates or by a threshold function multiplied by an exponential function, $a\sqrt{\Delta m - m_\pi} \cdot e^{b(\Delta m - m_\pi)}$, for the D^{*+} background. Since the invariant-mass resolution does not exhibit any dependence on $\Delta\varphi$ or q_2, the width of the Gaussian, for each D-meson species and p_T interval, was fixed to that obtained from a fit to the invariant-mass distribution integrated over $\Delta\varphi$ and q_2, where the signal has higher statistical significance.
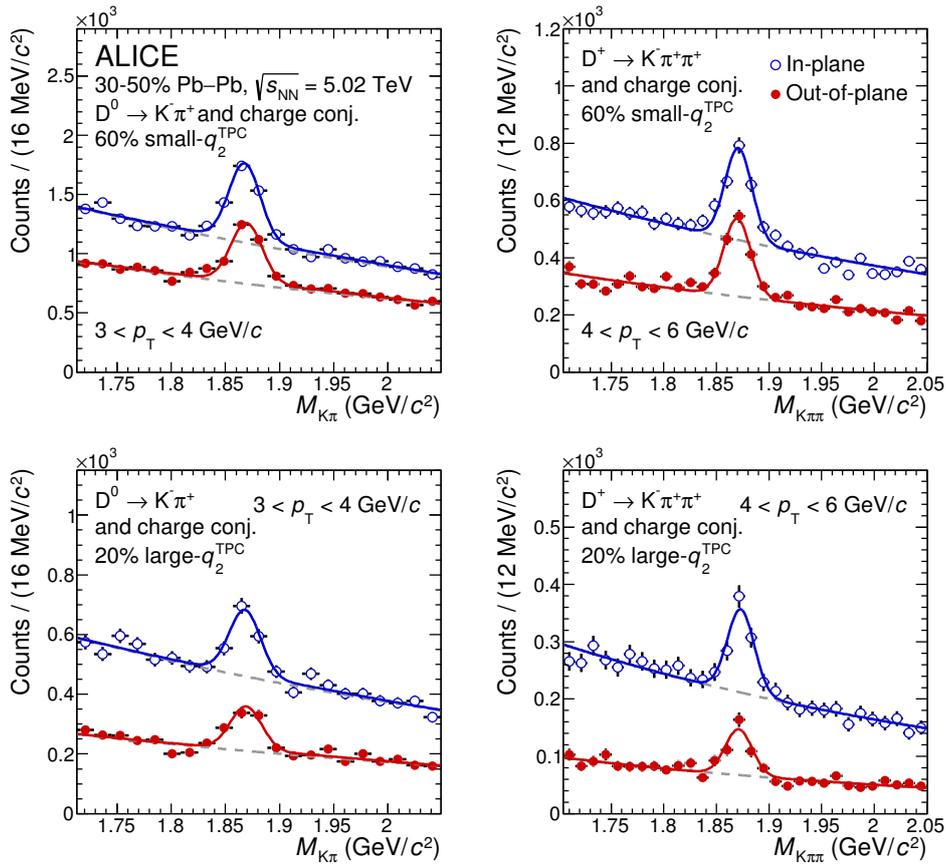
Figure 3: Invariant-mass distributions of D^0 candidates (left column) and D^+ candidates (right column) in two p_T intervals for the two $\Delta\varphi$ regions used in the EP method for the 30–50% Pb–Pb collisions at $\sqrt{s_{NN}} = 5.02$ TeV. The top row shows the distributions for the small-q_2^{TPC} sample, while the bottom row for the large-q_2^{TPC} sample (see text for details). The solid curves represent the total fit functions and the dotted curves the background functions, as described in the text.

In addition, for the determination of the D^0-meson yield, the contribution of signal candidates present in the invariant-mass distribution with the wrong K-π mass assignment was taken into account by including an additional term in the fit function, parametrised with a double-Gaussian shape [45] determined with Monte Carlo simulations. The contribution of the reflected signal, 2–5% under the D^0-peak region depending on p_T, was considered as background and therefore not included in the raw yield. Examples of invariant-mass fits for the three D-meson species in the unbiased sample in the 10–30% centrality class and for D^0 and D^+ mesons in the ESE-selected samples in the 30–50% centrality class are shown in Fig. 2 and Fig. 3, respectively.

The measured raw D-meson yields contain a feed-down contribution which, depending on the D-meson species, p_T and the topological selections, can vary between 5% and 20%. The strategy adopted to correct the observed v_2 for the fraction of prompt D mesons in the measured raw yields is the same as the one used in [48], and it is described in the following. The observed v_2 can be expressed as a linear combination of the prompt (D mesons coming directly from the hadronisation of a c-quark or from the decay of an excited open charm or charmonium state) and the feed-down contributions

$$v_2^{obs} = f_{prompt} v_2^{prompt} + (1 - f_{prompt}) v_2^{feed\text{-}down},$$
(6)

where f_{prompt} is the fraction of promptly produced D mesons estimated as a function of p_T with the same method used in [32]. In particular, it is computed using (i) FONLL calculations [85, 86] for the

production cross-section of beauty hadrons, (ii) the beauty-hadron decay kinematics from the EvtGen package [87], (iii) the product of efficiency and acceptance (Acc $\times$ ε) from Monte Carlo simulations and (iv) an hypothesis on the nuclear modification factor of feed-down D mesons. The nuclear modification factor is defined as $R_{\mathrm{AA}} = (\mathrm{d}N_{\mathrm{AA}}/\mathrm{d}p_{\mathrm{T}})/(\langle T_{\mathrm{AA}} \rangle \mathrm{d}\sigma_{pp}/\mathrm{d}p_{\mathrm{T}})$, where $\mathrm{d}N_{\mathrm{AA}}/\mathrm{d}p_{\mathrm{T}}$ and $\mathrm{d}\sigma_{pp}/\mathrm{d}p_{\mathrm{T}}$ are the p_{T}-differential yield and production cross section of D mesons in nucleus–nucleus (AA) and pp collisions, respectively, and $\langle T_{\mathrm{AA}} \rangle$ is the average nuclear overlap function in the considered centrality class [77]. The hypothesis $R_{\mathrm{AA}}^{\mathrm{feed\text{-}down}} = 2R_{\mathrm{AA}}^{\mathrm{prompt}}$ was used to estimate the central value of f_{prompt}. This choice is motivated by the comparison of the R_{AA} of prompt D mesons at $\sqrt{s_{\mathrm{NN}}} = 2.76$ TeV [88] with that of J/ψ from beauty-hadron decays at the same energy measured by the CMS Collaboration [30], which indicates that the charm-hadron production yield is more suppressed than that of the beauty hadrons by about a factor of two. This difference is described by model calculations with parton-mass-dependent energy loss [53]. The selection efficiency and therefore f_{prompt} are different in the 10–30% and 30–50% centrality classes, because of the different geometrical selections applied on the displaced decay-vertex topology. In the case of the ESE selection, the (Acc $\times$ ε) is the same for the large-q_2 and small-q_2 samples, because the same selection criteria were used in the two ESE-selected classes and the efficiency was found not to depend on local particle density. Therefore, considering also the same $R_{\mathrm{AA}}^{\mathrm{feed\text{-}down}}$ hypothesis, f_{prompt} resulted to be equal for the two ESE-selected classes and the unbiased sample in the same centrality interval. The uncertainties arising from the FONLL calculation, as well as the variation of the hypothesis on the $R_{\mathrm{AA}}^{\mathrm{feed\text{-}down}}$ in the interval $1 < R_{\mathrm{AA}}^{\mathrm{feed\text{-}down}}/R_{\mathrm{AA}}^{\mathrm{prompt}} < 3$, were taken into account as systematic uncertainties. The range of variation of $R_{\mathrm{AA}}^{\mathrm{feed\text{-}down}}/R_{\mathrm{AA}}^{\mathrm{prompt}}$ takes into account the data uncertainties and model variations. The elliptic flow of promptly produced D mesons was obtained assuming $v_2^{\mathrm{feed\text{-}down}} = v_2^{\mathrm{prompt}}/2$ and considering a flat probability distribution of $v_2^{\mathrm{feed\text{-}down}}$ in the interval $[0, v_2^{\mathrm{prompt}}]$. This hypothesis was suggested by the measurement of the non-prompt J/ψ v_2 in Pb–Pb collisions at $\sqrt{s_{\mathrm{NN}}} = 2.76$ TeV performed by the CMS Collaboration [30] and by the available models [50, 89, 90], that indicate $0 < v_2^{\mathrm{feed\text{-}down}} < v_2^{\mathrm{prompt}}$. As a consequence, the systematic uncertainty on v_2^{prompt} related to the feed-down subtraction is estimated by varying the central value of $v_2^{\mathrm{feed\text{-}down}}$ by $\pm v_2^{\mathrm{prompt}}/\sqrt{12}$, corresponding to ± 1 standard deviation of the assumed uniform distribution.

2.1 Non-flow contamination and q_2 selectivity

The possible effect of non-flow correlations between the D mesons and the charged particles used in the q_2 determination was investigated by comparing the v_2 values obtained with the ESE selection based on q_2^{TPC} to that obtained by selecting the events according to q_2^{V0A}. A difference in the results obtained using q_2^{TPC} and q_2^{V0A} can be attributed to different contributions of non-flow correlations, but also to the different eccentricity discriminating power of q_2 measured with the two detectors. This discriminating power depends on the magnitude of the elliptic flow, on the multiplicity used in the q_2 calculation and on the performance of the detector (i.e. the angular resolution or the linearity of the response as a function of charged-particle multiplicity). To disentangle the two effects, the selectivity of q_2^{TPC} was artificially reduced by rejecting randomly 85% of tracks used for the calculation of q_2^{TPC}. A similar strategy was used in [62]. Figure 4 illustrates the comparison of the effect of the ESE selection on the D^0-meson v_2 obtained using q_2^{TPC} (left-hand panels), q_2^{TPC} with random rejection of 85% of the tracks (middle panels) and q_2^{V0A} (right-hand panels), for the 10–30% (top panels) and the 30–50% (bottom panels) centrality classes. The separation between the measurements in the ESE-selected sample with respect to the unbiased one is reduced in the case of the random rejection of the tracks with respect to the default q_2^{TPC}, confirming the reduced q_2^{TPC} selectivity. The results obtained with q_2^{V0A} are similar to those obtained reducing artificially the selectivity of q_2^{TPC}, although they are compatible within uncertainties with both q_2^{TPC} measurements. This indicates that the statistical precision of the measurement is not sufficient to draw a firm conclusion about non-flow contaminations in the measurement performed by selecting the events according to q_2^{TPC}. The q_2^{TPC}-based selection was thus chosen for the evaluation of the results presented in the following sections, except for the comparison of the effect of the ESE selection on the D-mesons and the charged-particle v_2, for which the q_2^{V0A}-based selection was used.

9
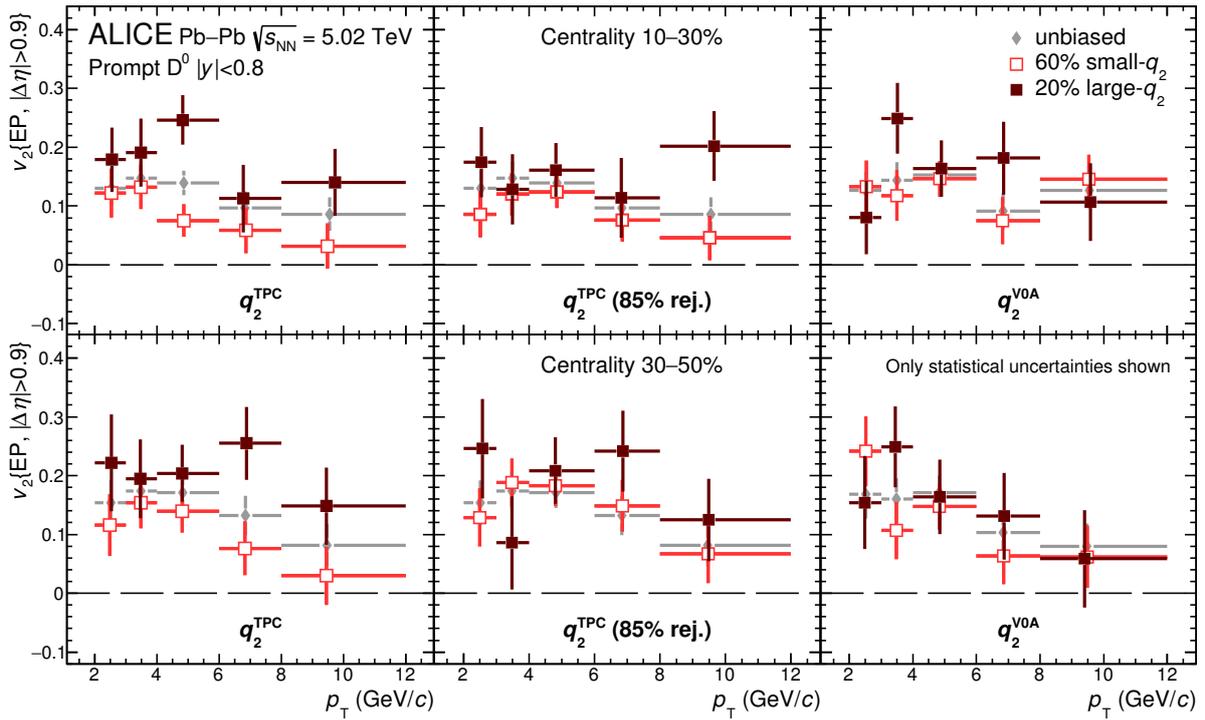
Figure 4: Comparison between the D^0 v_2 values measured in the unbiased sample and in the two event-shape classes obtained using TPC and V0A to compute q_2, for the 10–30% (top row) and 30–50% (bottom row) centrality classes. Only statistical uncertainties are shown.

3 Systematic uncertainties

The values of v_2 are affected by systematic uncertainties related to (i) the signal extraction from the invariant-mass distributions, (ii) the correction for the beauty feed-down contribution, (iii) the presence of non-flow effects, and (iv) the centrality dependence of the event-plane resolution correction R_2.

The uncertainty on the D-meson raw yield extraction from the invariant-mass distributions of candidates in the in-plane and out-of-plane azimuthal angle intervals was estimated with a multi-trial approach by repeating the fits several times with different configurations. In particular, the lower and upper limits of the fit range and the background fit function were varied, while the Gaussian width was kept fixed to the one extracted from the fits to the invariant mass distributions integrated over q_2 and $\Delta\varphi$. For each fit configuration, the D-meson v_2 was calculated from the in-plane and out-of-plane yields. The absolute systematic uncertainties were assigned as the r.m.s. of the v_2 distribution resulting from the different fits. They range from 0.005 to 0.040 in the 30–50% centrality class and from 0.008 to 0.040 in the 10–30% centrality class, depending on the p_T interval and the D-meson species. Further checks on the stability of the results were performed by repeating the procedure leaving the Gaussian width as a free parameter in the fits and by using a bin-counting method for the definition of the raw yield. With the latter method, the signal yield was obtained by counting the histogram entries in the invariant-mass region of the signal ($|M - M_{\text{peak}}| < 3.5\sigma$), after subtracting the background contribution estimated from a fit to the side bands ($|M - M_{\text{peak}}| > 4\sigma$). The v_2 values obtained from these checks were found to be within the uncertainty estimated by varying the fit conditions and therefore no additional systematic uncertainty was assigned. For the analysis with ESE selection, further studies were carried out by comparing the output of the multiple-trial fit procedure described above in the small-q_2, large-q_2 and q_2-integrated samples for each of the tested fit configurations. These checks indicated that this contribution to the systematic uncertainty is uncorrelated between the event samples selected based on the q_2 value.

The contribution of the beauty feed-down correction to the systematic uncertainty was estimated varying (i) the quark mass and the renormalisation and factorisation scales in the FONLL calculations; (ii) the $R_{\mathrm{AA}}^{\mathrm{feed\text{-}down}}$ hypothesis; and (iii) the $v_2^{\mathrm{feed\text{-}down}}$ hypothesis as described in Sec. 2. The value of the corresponding absolute systematic uncertainty ranges from 0.001 to 0.030 depending on the D-meson species and p_{T} as well as on the ESE-selected class.

The systematic uncertainty on the event-plane resolution correction factor R_2 has two contributions, which are common to the unbiased, small-q_2 and large-q_2 samples. The first one originates from possible non-flow effects affecting the estimation of R_2, when the particles reconstructed in the two semivolumes of the TPC are used as sub-events. It was estimated by comparing the value of R_2 obtained by introducing two different pseudorapidity gaps ($\Delta\eta = 0.2$ and $\Delta\eta = 0.4$) between the sub-events of the TPC tracks with positive/negative η. The second contribution is due to the centrality dependence of R_2 within the classes used in the analysis. The central value of R_2 was computed from the three sub-event correlations averaged over the events in the 10–30% and 30–50% intervals. The uncertainty was estimated by comparing this value with those obtained as weighted averages of the R_2 values in narrow centrality intervals, using as weights either the D-meson yields or the average number of nucleon–nucleon collisions. A systematic uncertainty of 2% on R_2 was assigned based on these studies for all centrality and ESE-selected classes.

For the ESE-selected samples, an additional bias on the resolution correction factor can originate from autocorrelations because of the usage of TPC tracks (V0A signals) for both q_2^{TPC} (q_2^{V0A}) and R_2 determination. In particular, the selection on q_2^{TPC} can bias the correlation between the sub-events of charged particles reconstructed in the TPC with $0 < \eta < 0.8$ and with $-0.8 < \eta < 0$ used in the three sub-event calculation of R_2. To estimate this systematic uncertainty, an alternative approach to compute R_2 was utilised, which is based on (i) the correlations between the sub-events reconstructed with the V0 and half of the TPC tracks (with $\eta < 0$) and (ii) the assumption that the ratio of the variables χ_{V0} and $\chi_{\mathrm{TPC},\eta<0}$ governing the event plane resolution (see Ref. [35] for its definition) is the same in the unbiased and ESE-selected samples. The difference between the R_2 values obtained with this approach and the three sub-event method, which amounts to 3% and 5% in the 10–30% and 30–50% centrality classes, respectively, was assigned as systematic uncertainty on the ESE-selected samples. The same procedure was adopted for the samples selected using the q_2^{V0A}. In this case, the systematic uncertainty was estimated to be of the order of 1% for the large-q_2^{V0A} sample, while negligible for the small-q_2^{V0A} sample, for both the centrality classes.

As discussed in Sec. 2.1, a further bias in the analyses with q_2^{TPC}-based selection could be induced by non-flow correlations between the D meson and the sample of tracks used for the q_2 measurement, which can include charged particles originating from the fragmentation of the charm quarks. To further study this effect, the analysis with q_2^{TPC}-based selection was repeated introducing a "jet-veto" pseudorapidity gap of $|\Delta\eta| = 0.1$ units between each D-meson candidate and the tracks used to measure q_2^{TPC}. Since no significant difference was observed, no systematic uncertainty was assigned.

4 Results

In Fig. 5 the elliptic flow coefficient v_2 of prompt D^0, D^+, and D^{*+} mesons is reported as a function of p_{T} in the centrality class 10–30%. The symbols are positioned at the average p_{T} of the reconstructed D mesons, which is determined as the average of the p_{T} distribution of candidates in the signal invariant-mass region, after subtracting the contribution of the background candidates estimated from the side bands. The systematic uncertainty of the feed-down correction is displayed separately in the figure. The v_2 of D^0, D^+ and D^{*+} mesons is consistent among the various species and larger than zero in the interval $2 < p_{\mathrm{T}} < 8$ GeV/c.

The average v_2 and p_{T} of prompt D^0, D^+, D^{*+} mesons as a function of p_{T} was computed by using the
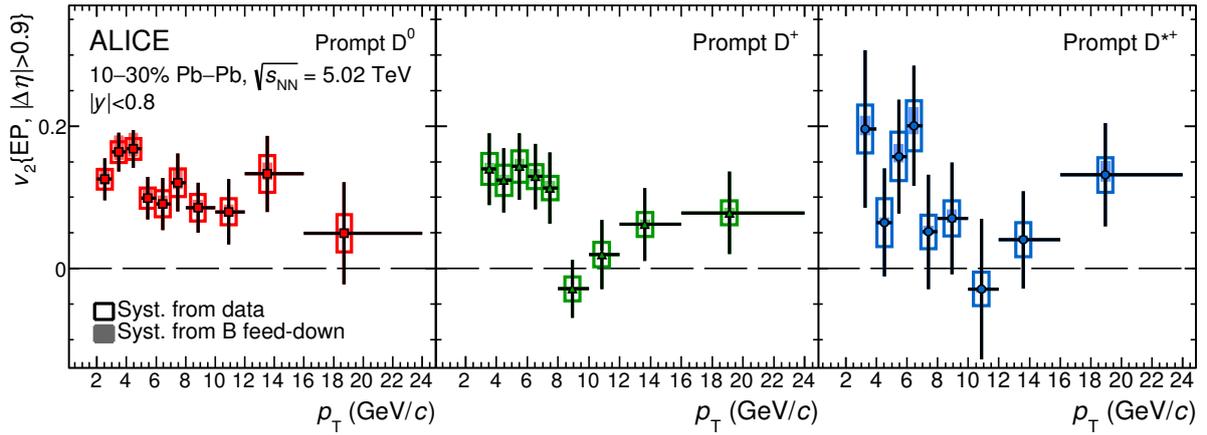
Figure 5: Elliptic flow coefficient v_2 as a function of p_T for prompt D^0, D^+, and D^{*+} mesons for Pb–Pb collisions at $\sqrt{s_{NN}} = 5.02$ TeV in the centrality class 10–30%. The symbols are positioned horizontally at the average p_T of the reconstructed D mesons. Vertical error bars represent the statistical uncertainty, empty boxes the systematic uncertainty associated with the D-meson anisotropy measurement and the event-plane resolution. Shaded boxes show the uncertainty due to the feed-down from beauty-hadron decays.

inverse of the squared absolute statistical uncertainties as weights and is reported in the left panel of Fig. 6. The systematic uncertainties were propagated by considering the contribution from the event-plane resolution R_2 and the feed-down correction as correlated among the D-meson species. In the right panel of Fig. 6, the average v_2 of D^0, D^+, and D^{*+} as a function of p_T in the centrality class 30–50% taken from [48] is reported. The measurements in both centrality classes are compatible within uncertainties with the D^0-meson v_2 measured with the Scalar Product (SP) method [69, 78] by the CMS Collaboration in $|y| < 1$ [49]. The charged-pion v_2 measured in $|y| < 0.5$ by the ALICE Collaboration using the SP method [91] is also superimposed for comparison. The D-meson v_2 is similar in magnitude to that of $\pi^\pm$ for $4 < p_T < 10$ GeV/c. In the region $p_T < 4$ GeV/c, where a mass ordering for light hadrons is observed and described by hydrodynamical calculations [92], the values of the D-meson v_2 are slightly
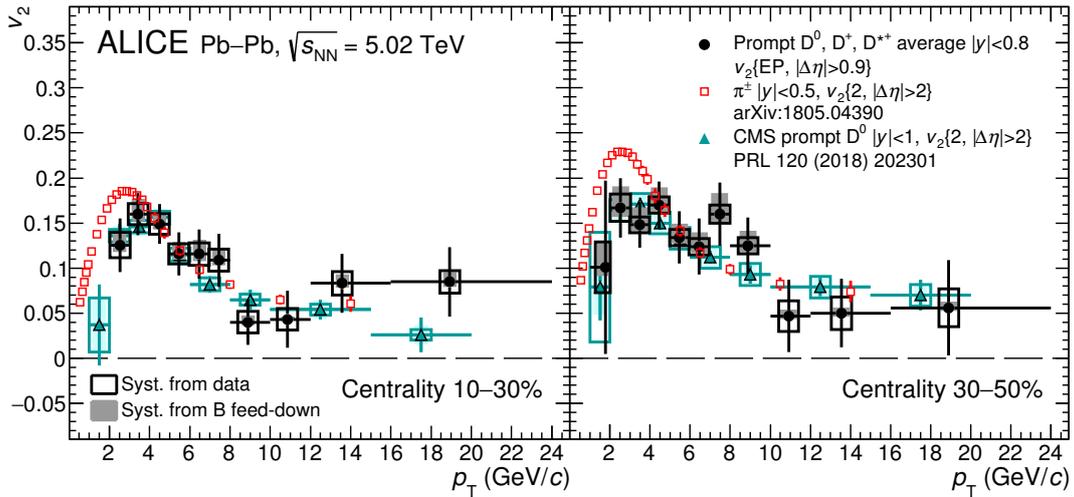
Figure 6: Average D^0, D^+, D^{*+} v_2 as a function of p_T for Pb–Pb collisions at $\sqrt{s_{NN}} = 5.02$ TeV in the centrality classes 10–30% (left) and 30–50% [48] (right). The comparison with the measurement of the D^0 v_2 by the CMS Collaboration [49] and the charged pion v_2 [91] in the same centrality intervals is also shown.
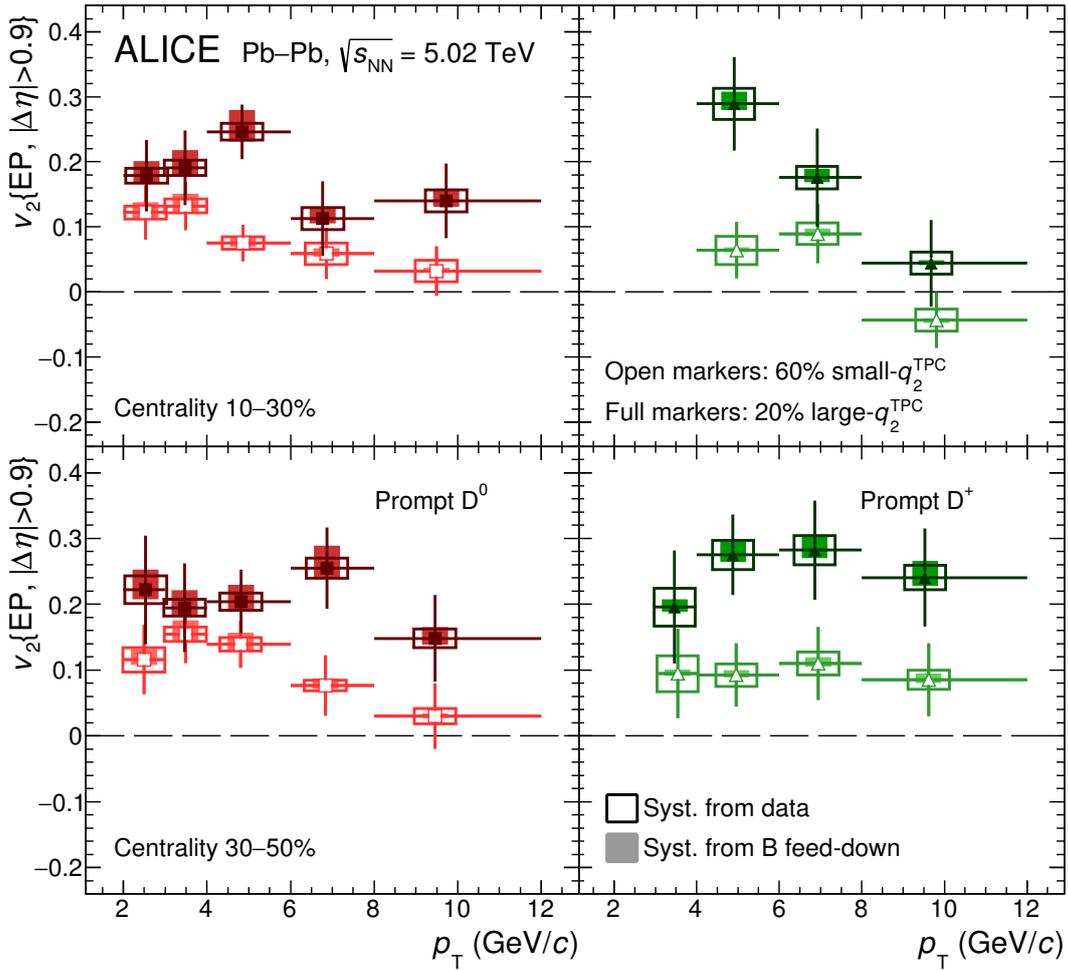
Figure 7: D^0 (left column) and D^+ (right column) v_2 as a function of p_T for the small-q_2^{TPC} and large-q_2^{TPC} samples (see text for details), in Pb–Pb collisions at $\sqrt{s_{NN}} = 5.02$ TeV in the 10–30% (top row) and 30–50% (bottom row) centrality classes. The symbols are positioned horizontally at the average p_T of the reconstructed D mesons. Vertical error bars represent the statistical uncertainty, empty boxes the systematic uncertainty associated with the D-meson anisotropy measurement and the event-plane resolution. Shaded boxes show the uncertainty due to feed-down from beauty-hadron decays.

lower than those of $\pi^\pm$, but compatible within uncertainties.

Figure 7 shows the prompt D^0 and D^+ v_2 as a function of p_T in the small-q_2^{TPC} and large-q_2^{TPC} samples, in the centrality classes 10–30% (top row) and 30–50% (bottom row). The measurement of the D^{*+} v_2 in the ESE-selected samples was not possible due to the small statistical significance, while the measurements of D^0 and D^+ mesons were performed in wider p_T intervals compared to the unbiased v_2 measurement and in the reduced range $2 < p_T < 12$ GeV/c, due to the limited size of the data sample. The measurements of the v_2 of the two different D-meson species in the ESE-selected classes are compatible with each other within uncertainties. Also in this case, the symbols are positioned at the average D-meson p_T determined as described above.

The average v_2 of D^0 and D^+ mesons has been calculated in the small-q_2^{TPC} and large-q_2^{TPC} samples with the same weighted average procedure described above. It is shown for the two considered centrality classes in the top panels of Fig. 8 together with the v_2 measured in the unbiased sample, recalculated in the same p_T intervals of the ESE analysis. In the bottom panels of the same figure, the ratio of the average
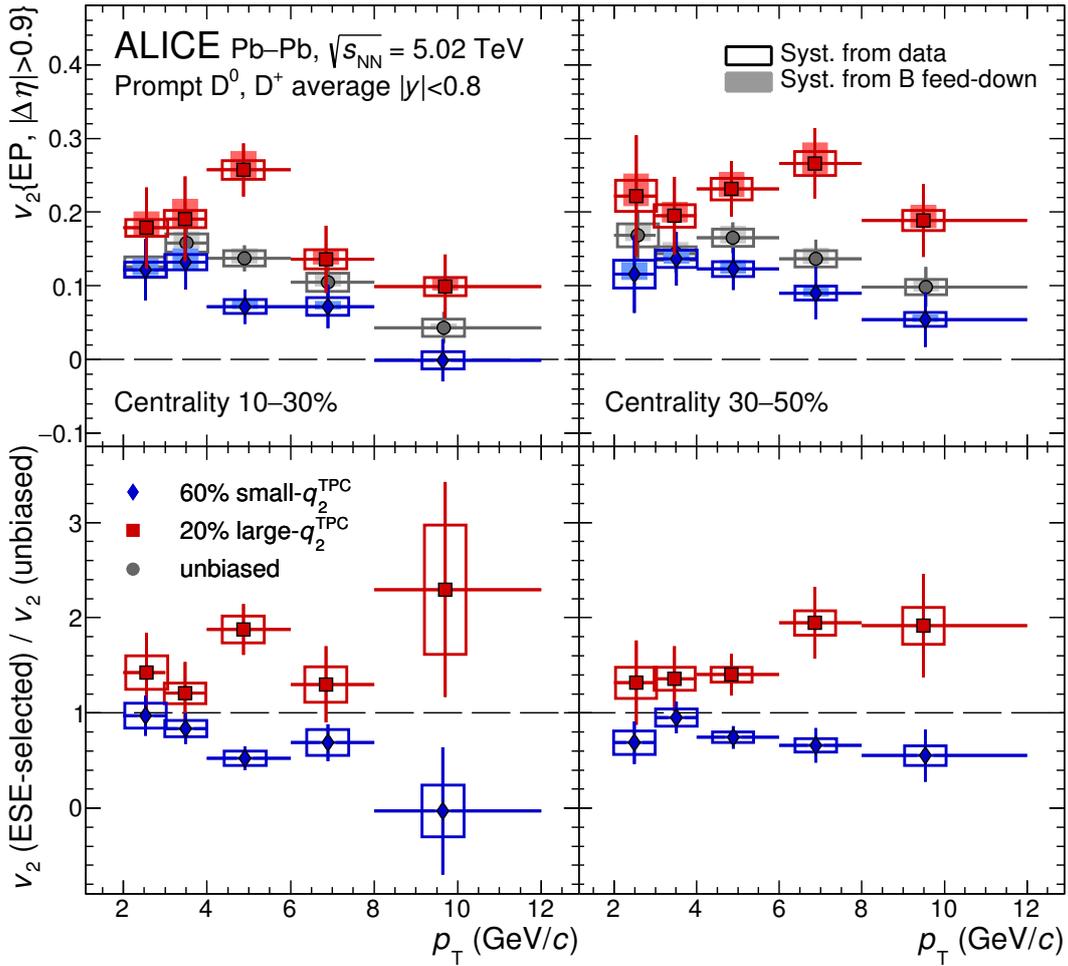
Figure 8: Top panels: average of D^0 and D^+ v_2 as a function of p_T for Pb–Pb collisions at $\sqrt{s_{NN}} = 5.02$ TeV in the small-q_2^{TPC}, large-q_2^{TPC} (see text for details) and unbiased samples, in the 10–30% (left) and 30–50% (right) centrality classes. Bottom panels: ratios of the measured v_2 in the ESE-selected classes to the one obtained from the unbiased sample.

D-meson v_2 from the ESE-selected samples with respect to that of the unbiased samples is illustrated. The statistical uncertainties on the ratio were propagated taking into account the degree of correlation between the measured yields in the small-q_2^{TPC} (large-q_2^{TPC}) and the unbiased sample. The systematic uncertainties were propagated considering the contribution from the centrality dependence and the non-flow contaminations among sub-events of R_2 as well as the feed-down correction as correlated between the measurements in the ESE-selected and the unbiased samples.

The observation of a flat ratio as a function of p_T for light hadron v_2 with ESE-selection at $\sqrt{s_{NN}} = 2.76$ TeV indicated that the q_2 value is connected to a global property of the event [62]. For D mesons, the modification of the v_2 in the q_2^{TPC}-selected samples is compatible within uncertainties with a flat behaviour as a function of p_T for both the 10–30% and the 30–50% centrality classes. However, the current precision of the measurement does not allow to exclude a p_T dependence which would indicate the presence of non-flow contaminations.

Selecting the 20% (60%) highest (lowest) q_2^{TPC} sample leads to a change of about 40% (25%) in the measured v_2. The corresponding variation of the average q_2^{TPC} in the ESE-selected classes was found to be about 65% and 30% in the large-q_2^{TPC} and small-q_2^{TPC} samples, respectively. The increase
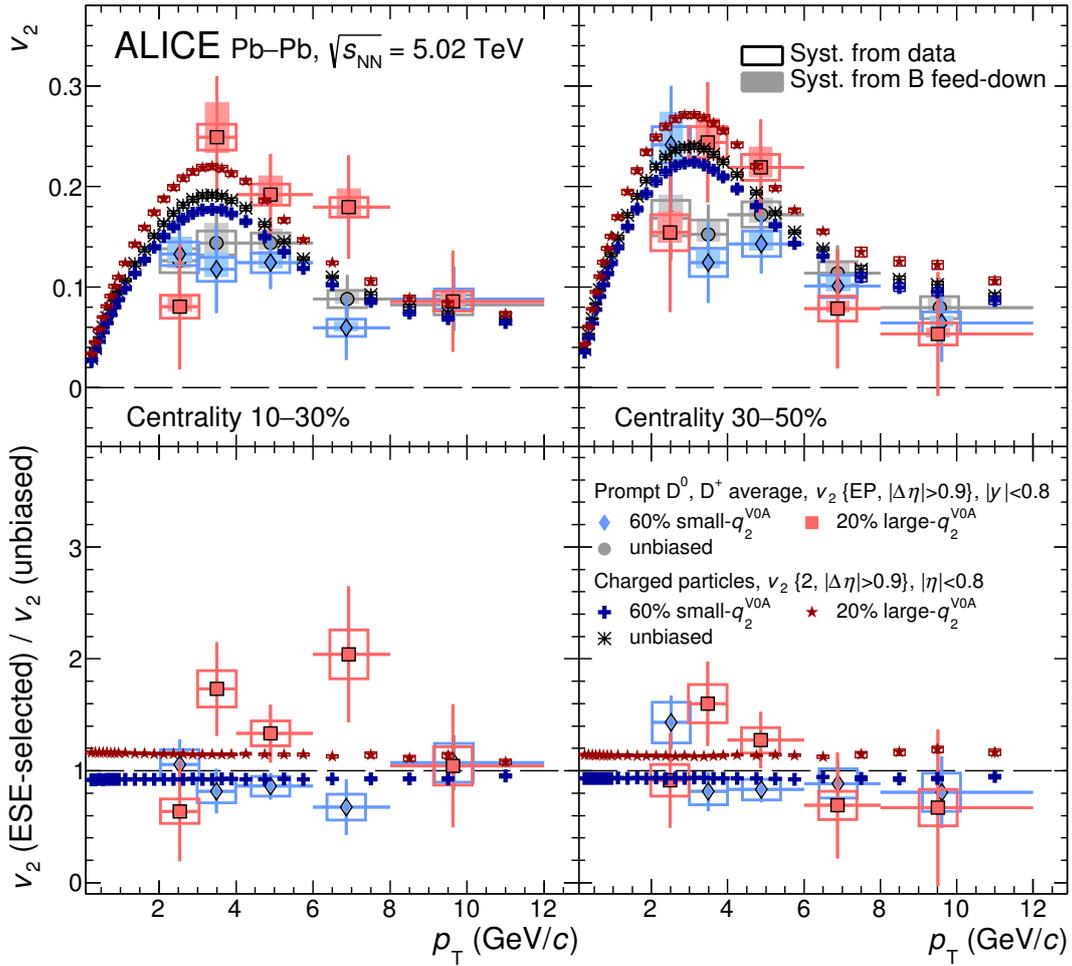
Figure 9: Top panels: average of D^0 and D^+ v_2 as a function of p_T for Pb–Pb collisions at $\sqrt{s_{NN}} = 5.02$ TeV in the small-q_2^{V0A}, large-q_2^{V0A} (see text for details) and unbiased samples, in the 10–30% (left) and 30–50% (right) centrality classes. The charged-particle v_2 obtained at the same energy, centrality classes and ESE samples are superimposed for comparison. Bottom panels: ratios of the measured v_2 in the ESE-selected classes to the one obtained from the unbiased sample.

(decrease) of the D-meson v_2 and the average q_2^{TPC} observed in the large-q_2^{TPC} (small-q_2^{TPC}) sample with respect to the unbiased one is similar within uncertainties in the two centrality intervals considered. Considering as null hypothesis $v_2(\text{large-}q_2^{TPC}) = v_2(\text{small-}q_2^{TPC})$, the probability to observe the measured positive $\Delta v_2 = v_2(\text{large-}q_2^{TPC}) - v_2(\text{small-}q_2^{TPC})$ in the full p_T range of the measurement, corresponds to a significance of about 4σ, taking into account both statistical and systematic uncertainties in each centrality class. It is however important to keep in mind that part of the observed effect could be slightly enlarged by non-flow contaminations, as previously mentioned.

The effect of the ESE selection on the D-meson v_2 was compared to that observed for charged particles. For this comparison, the ESE selection was performed using q_2^{V0A}, in order to avoid autocorrelations and non-flow contaminations. In the top panels of Fig. 9, the average D^0 and D^+ v_2 in the ESE-selected and unbiased samples in the 10–30% (left panel) and 30–50% (right panel) centrality classes are depicted together with the charged-particle v_2 measured at the same energy, centrality classes and ESE-selected samples. The charged-particle v_2 was measured with the SP method considering reconstructed tracks with $|\eta| < 0.8$ and $0.2 < p_T < 12$ GeV/c, selected as in Ref. [91]. The bottom panels of the same
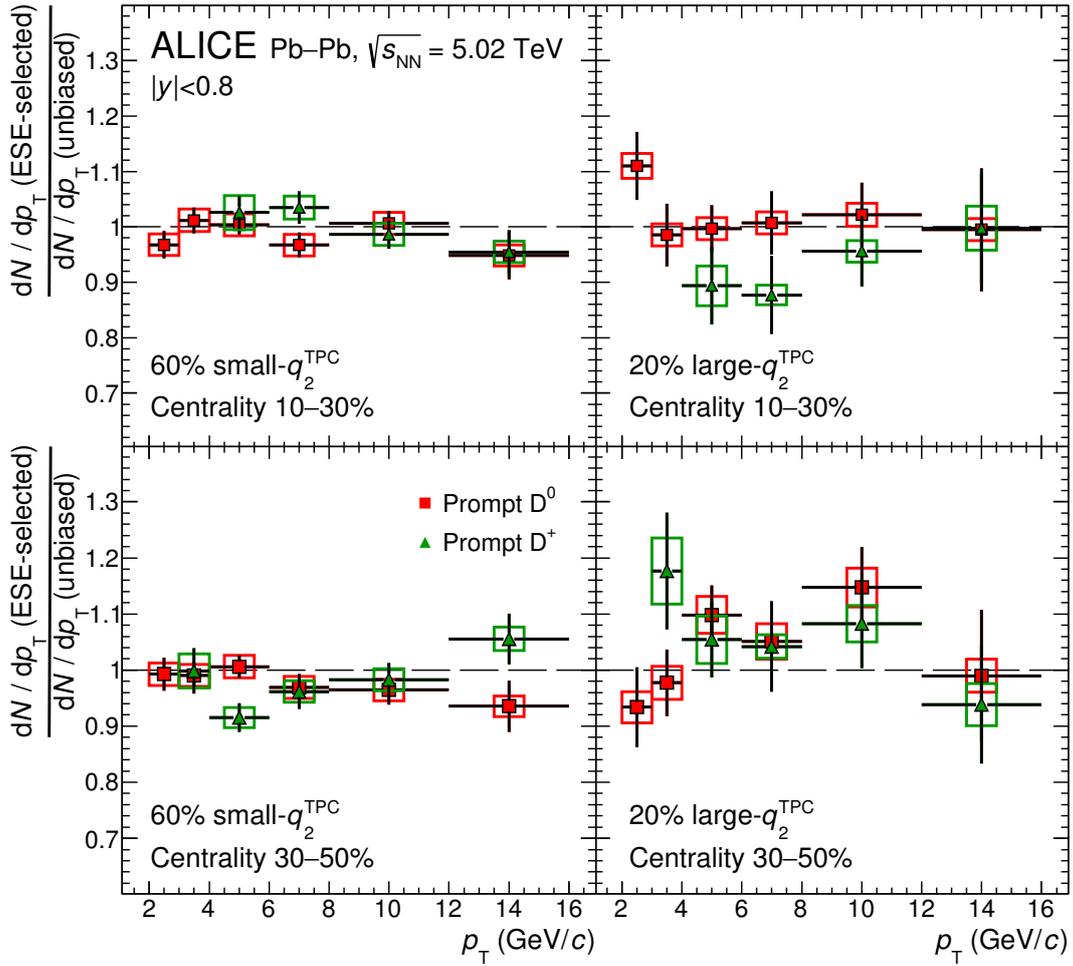
Figure 10: Ratio of the yields of D^0 and D^+ mesons measured as a function of p_T in the small-q_2^{TPC} (left column) and large-q_2^{TPC} (right column) samples (see text for details) to that in the unbiased sample, in Pb–Pb collisions at $\sqrt{s_{NN}} = 5.02$ TeV for the 10–30% (top row) and 30–50% (bottom row) centrality classes. Vertical error bars represent the statistical uncertainty, empty boxes the total systematic uncertainty.

figure show the ratios of the v_2 measured in the ESE-selected samples with respect to the unbiased one. The ratios between the charged-particle v_2 show almost no p_T dependence, confirming that the usage of the q_2^{V0A} provides a selection of a global property of the collision. The relative variation of the charged-particle v_2 in the large-q_2^{V0A} and small-q_2^{V0A} samples was found to be of about 14-15% and 7-8%, respectively. These values reflect the reduced sensitivity of the ESE selection obtained using the V0A with respect to that based on TPC tracks. The ratios of the average D-meson v_2 in the ESE-selected samples with respect to the unbiased one were found to be compatible within uncertainties with those of charged particles in the corresponding samples, suggesting that the response to the ESE selection is similar for D mesons and the bulk of light hadrons. However, given the reduced selectivity of q_2^{V0A} and the current experimental uncertainties, the ratios of the average D-meson v_2 are also compatible with unity, and therefore a firm conclusion cannot be drawn. Nevertheless, the comparison between D mesons and charged particles will be crucial for future larger data samples, to better asses the magnitude of the correlation between the D-meson and the soft-hadron v_2.

To study a possible interplay between the azimuthal anisotropy of the event and the charm-quark radial flow (at low/intermediate p_T) and in-medium energy loss (at high p_T), the yields of prompt D^0 and D^+
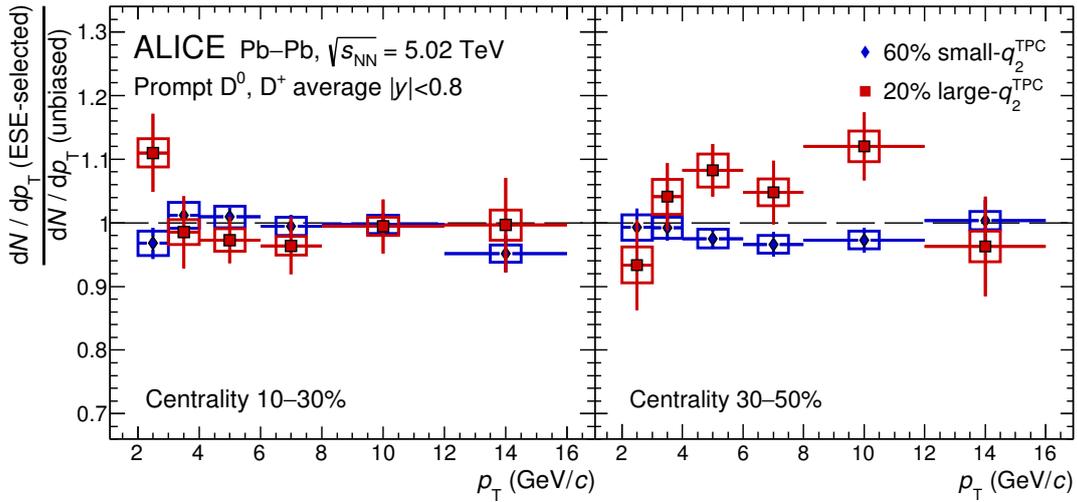
Figure 11: Average of the ratio of D^0 and D^+ yields measured as a function of p_T in the ESE-selected samples to those in the unbiased sample, in Pb–Pb collisions at $\sqrt{s_{NN}} = 5.02$ TeV for the 10–30% (left panel) and 30–50% (right panel) centrality classes. Vertical error bars represent the statistical uncertainty, empty boxes the total systematic uncertainty.

mesons have been measured in six transverse momentum intervals in the range $2 < p_T < 16$ GeV/c, in the small-q_2^{TPC} and large-q_2^{TPC} samples.

The D-meson raw yields integrated over $\Delta\varphi$ were extracted from the fits to the invariant-mass distributions in the ESE-selected and unbiased classes and normalised to the corresponding number of events in the considered sample. As described in Sec. 2, the selection and reconstruction efficiencies of prompt D mesons do not show any dependence on q_2 within the ESE selections considered in this analysis, therefore no correction to the raw yields was applied. The fraction of prompt D mesons, f_{prompt}, was estimated using the same strategy adopted for the v_2 measurement and it is the same in the ESE-selected and the unbiased samples.

The ratio of the D-meson yields in the small-q_2^{TPC} (large-q_2^{TPC}) sample to those in the unbiased sample are shown in Fig. 10 as a function of p_T in the 10–30% (top row) and 30–50% (bottom row) centrality classes. The systematic uncertainty on the raw D-meson yield extraction was evaluated directly on the ratio of the yields, applying the same strategy used for the v_2 (see Sec. 3). The systematic uncertainty on the reconstruction and selection efficiency, arising from a possible imperfect description of the data in the Monte Carlo simulations, cancels out in the ratio, since the efficiency is the same in the two ESE-selected classes.

The average of the ratio of the D^0 and D^+ yields in the small-q_2^{TPC} (large-q_2^{TPC}) sample to those in the unbiased sample is depicted in Fig. 11. It was computed by using the inverse of the squared relative statistical uncertainties as weights.

In the 10–30% centrality class, the ratio between the D-meson yields in ESE-selected samples to those in the unbiased sample was found to be compatible with unity in the measured p_T range. In the 30–50% centrality class, the central values of the D-meson per-event yields in the large-q_2^{TPC} (small-q_2^{TPC}) samples were found to be higher (lower) than those in the unbiased sample in all the measured p_T intervals in the range $3 < p_T < 12$ GeV/c. However, the ratios between the yields in the ESE-selected samples to the unbiased yields are compatible with unity within about one standard deviation.

In the light-hadron sector, the effect induced by the correlation between radial and elliptic flow, attributed to a larger initial density in more anisotropic events, was observed to be of the order of 5% for charged

pions with $p_T \approx 4$ GeV/c in mid-central Pb–Pb collisions at $\sqrt{s_{\mathrm{NN}}} = 2.76$ TeV [62]. Since the ratio between the D-meson yields in ESE-selected samples to those in the unbiased sample was found to be compatible with unity, a possible similar effect is expected to be smaller than the present experimental uncertainties, which do not allow for any conclusion.

5 Summary

The first application of the event-shape engineering technique to the measurement of D-meson production in Pb–Pb collisions at $\sqrt{s_{\mathrm{NN}}} = 5.02$ TeV has been presented.

The elliptic flow of D^0, D^+, and D^{*+} mesons at mid-rapidity in the 10–30% (30–50%) centrality class was measured with the event-plane technique and found to be larger than zero in the transverse momentum interval $2 < p_T < 8(10)$ GeV/c and similar in magnitude to that of charged pions for $p_T > 4$ GeV/c, while slightly lower for $p_T < 4$ GeV/c, in the same centrality class.

The v_2 coefficient of D^0 and D^+ mesons was measured in events with different magnitude of the average bulk elliptic flow, quantified by the value of q_2 measured using TPC tracks to maximise the selectivity. The observation of a larger (smaller) D-meson v_2 in events with large-q_2^{TPC} (small-q_2^{TPC}) values confirms a correlation between D-meson azimuthal anisotropy and the collective expansion of the bulk of light hadrons. When using the V0A to measure q_2 in order to reduce non-flow contaminations and autocorrelations, the variation of the D-meson v_2 in the small-q_2^{V0A} and large-q_2^{V0A} samples was found to be compatible within uncertainties with that of charged particles, suggesting a similar response to the ESE selection.

The ratio of the p_T-differential yields measured in the ESE-selected samples with respect to those in the unbiased sample was found to be compatible with unity in both the 10–30% and 30–50% centrality classes, with a possible indication of larger D-meson yield for $3 < p_T < 12$ GeV/c in events with higher-than-average bulk elliptic flow in the 30–50% centrality class. With the current uncertainties no firm conclusion can be drawn on the possible interplay between the initial spatial anisotropy and the charm-quark energy loss and radial flow.

The measurements presented in this paper open the way to the study of heavy-quark production with the Event-Shape Engineering technique, which offers a new possibility to understand the correlation of heavy-quark and bulk properties. An improved precision is expected to be achieved with future data samples that will be collected in 2018 and during Run 3 and 4 of the LHC [93, 94].

References

[1] F. Karsch, "Lattice simulations of the thermodynamics of strongly interacting elementary particles and the exploration of new phases of matter in relativistic heavy ion collisions," *J. Phys. Conf. Ser.* **46** (2006) 122, arXiv:hep-lat/0608003 [hep-lat].

[2] **Wuppertal-Budapest** Collaboration, S. Borsanyi, Z. Fodor, C. Hoelbling, S. D. Katz, S. Krieg, C. Ratti, and K. K. Szabo, "Is there still any T_c mystery in lattice QCD? Results with physical masses in the continuum limit III," *JHEP* **09** (2010) 073, arXiv:1005.3508 [hep-lat].

[3] **HotQCD** Collaboration, A. Bazavov *et al.*, "The chiral and deconfinement aspects of the QCD transition," *Phys. Rev.* **D85** (2012) 054503, arXiv:1111.1710 [hep-lat].

[4] W. Florkowski, R. Ryblewski, N. Su, and K. Tywoniuk, "Strong-coupling effects in a plasma of confining gluons," *Nucl. Phys.* **A956** (2016) 669–672, arXiv:1512.06402 [hep-ph].

[5] H. Song, S. A. Bass, U. Heinz, T. Hirano, and C. Shen, "200 A GeV Au+Au collisions serve a nearly perfect quark-gluon liquid," *Phys. Rev. Lett.* **106** (2011) 192301, arXiv:1011.2783

[nucl-th]. [Erratum: Phys. Rev. Lett.109,139904(2012)].

[6] Z. Qiu, C. Shen, and U. Heinz, "Hydrodynamic elliptic and triangular flow in Pb-Pb collisions at $\sqrt{s} = 2.76$ ATeV," *Phys. Lett.* **B707** (2012) 151–155, arXiv:1110.3033 [nucl-th].

[7] C. Gale, S. Jeon, B. Schenke, P. Tribedy, and R. Venugopalan, "Event-by-event anisotropic flow in heavy-ion collisions from combined Yang-Mills and viscous fluid dynamics," *Phys. Rev. Lett.* **110** no. 1, (2013) 012302, arXiv:1209.6330 [nucl-th].

[8] **STAR** Collaboration, J. Adams *et al.*, "Azimuthal anisotropy in Au+Au collisions at $\sqrt{s_{\mathrm{NN}}} = 200$ GeV," *Phys. Rev.* **C72** (2005) 014904, arXiv:nucl-ex/0409033 [nucl-ex].

[9] **PHOBOS** Collaboration, B. Alver *et al.*, "System size, energy, pseudorapidity, and centrality dependence of elliptic flow," *Phys. Rev. Lett.* **98** (2007) 242302, arXiv:nucl-ex/0610037 [nucl-ex].

[10] **ALICE** Collaboration, K. Aamodt *et al.*, "Higher harmonic anisotropic flow measurements of charged particles in Pb–Pb collisions at $\sqrt{s_{\mathrm{NN}}}$=2.76 TeV," *Phys. Rev. Lett.* **107** (2011) 032301, arXiv:1105.3865 [nucl-ex].

[11] F.-M. Liu and S.-X. Liu, "Quark-gluon plasma formation time and direct photons from heavy ion collisions," *Phys. Rev.* **C89** no. 3, (2014) 034906, arXiv:1212.6587 [nucl-th].

[12] P. Braun-Munzinger, "Quarkonium production in ultra-relativistic nuclear collisions: Suppression versus enhancement," *J. Phys.* **G34** (2007) S471, arXiv:nucl-th/0701093 [NUCL-TH].

[13] A. Andronic *et al.*, "Heavy-flavour and quarkonium production in the LHC era: from proton-proton to heavy-ion collisions," *Eur. Phys. J.* **C76** (2016) 107, arXiv:1506.03981 [nucl-ex].

[14] G. Aarts *et al.*, "Heavy-flavor production and medium properties in high-energy nuclear collisions - What next?," *Eur. Phys. J.* **A53** no. 5, (2017) 93, arXiv:1612.08032 [nucl-th].

[15] M. Gyulassy and M. Plumer, "Jet Quenching in Dense Matter," *Phys. Lett.* **B243** (1990) 432.

[16] R. Baier, Y. L. Dokshitzer, A. H. Mueller, S. Peigne, and D. Schiff, "Radiative energy loss and p_{T} broadening of high-energy partons in nuclei," *Nucl. Phys.* **B484** (1997) 265, arXiv:hep-ph/9608322 [hep-ph].

[17] F. Prino and R. Rapp, "Open Heavy Flavor in QCD Matter and in Nuclear Collisions," *J. Phys.* **G43** (2016) 093002, arXiv:1603.00529 [nucl-ex].

[18] E. Braaten and M. H. Thoma, "Energy loss of a heavy quark in the quark - gluon plasma," *Phys. Rev.* **D44** (1991) R2625.

[19] V. Greco, C. M. Ko, and P. Levai, "Parton coalescence at RHIC," *Phys. Rev.* **C68** (2003) 034904, arXiv:nucl-th/0305024 [nucl-th].

[20] A. Andronic, P. Braun-Munzinger, K. Redlich, and J. Stachel, "Statistical hadronization of charm in heavy ion collisions at SPS, RHIC and LHC," *Phys. Lett.* **B571** (2003) 36, arXiv:nucl-th/0303036 [nucl-th].

[21] S. Plumari, V. Minissale, S. K. Das, G. Coci, and V. Greco, "Charmed Hadrons from Coalescence plus Fragmentation in relativistic nucleus-nucleus collisions at RHIC and LHC," *Eur. Phys. J.* **C78** no. 4, (2018) 348, arXiv:1712.00730 [hep-ph].

[22] **PHENIX** Collaboration, A. Adare *et al.*, "Heavy Quark Production in $p + p$ and Energy Loss and Flow of Heavy Quarks in Au+Au Collisions at $\sqrt{s_{\mathrm{NN}}} = 200$ GeV," *Phys. Rev.* **C84** (2011) 044905, arXiv:1005.1627 [nucl-ex].

[23] **STAR** Collaboration, B. I. Abelev *et al.*, "Transverse momentum and centrality dependence of high-p_T non-photonic electron suppression in Au+Au collisions at $\sqrt{s_{\mathrm{NN}}} = 200$ GeV," *Phys. Rev. Lett.* **98** (2007) 192301, arXiv:nucl-ex/0607012 [nucl-ex]. [Erratum: Phys. Rev. Lett.106 (2011) 159902].

[24] **STAR** Collaboration, L. Adamczyk *et al.*, "Observation of D^0 Meson Nuclear Modifications in

Au+Au Collisions at $\sqrt{s_{NN}} = 200$ GeV," *Phys. Rev. Lett.* **113** (2014) 142301, `arXiv:1404.6185` `[nucl-ex]`.

[25] **PHENIX** Collaboration, S. S. Adler *et al.*, "Nuclear modification of electron spectra and implications for heavy quark energy loss in Au+Au collisions at $\sqrt{s_{NN}} = 200$ GeV," *Phys. Rev. Lett.* **96** (2006) 032301, `arXiv:nucl-ex/0510047` `[nucl-ex]`.

[26] **ALICE** Collaboration, J. Adam *et al.*, "Transverse momentum dependence of D-meson production in Pb-Pb collisions at $\sqrt{s_{NN}} = 2.76$ TeV," *JHEP* **03** (2016) 081, `arXiv:1509.06888` `[nucl-ex]`.

[27] **ALICE** Collaboration, B. Abelev *et al.*, "Production of muons from heavy flavour decays at forward rapidity in pp and Pb-Pb collisions at $\sqrt{s_{NN}} = 2.76$ TeV," *Phys. Rev. Lett.* **109** (2012) 112301, `arXiv:1205.6443` `[hep-ex]`.

[28] **ALICE** Collaboration, J. Adam *et al.*, "Measurement of the production of high-p_T electrons from heavy-flavour hadron decays in Pb-Pb collisions at $\sqrt{s_{NN}} = 2.76$ TeV," *Phys. Lett.* **B771** (2017) 467–481, `arXiv:1609.07104` `[nucl-ex]`.

[29] **ALICE** Collaboration, J. Adam *et al.*, "Measurement of electrons from beauty-hadron decays in p-Pb collisions at $\sqrt{s_{NN}} = 5.02$ TeV and Pb-Pb collisions at $\sqrt{s_{NN}} = 2.76$ TeV," *JHEP* **07** (2017) 052, `arXiv:1609.03898` `[nucl-ex]`.

[30] **CMS** Collaboration, V. Khachatryan *et al.*, "Suppression and azimuthal anisotropy of prompt and nonprompt J/ψ production in PbPb collisions at $\sqrt{s_{NN}} = 2.76$ TeV," *Eur. Phys. J.* **C77** no. 4, (2017) 252, `arXiv:1610.00613` `[nucl-ex]`.

[31] **CMS** Collaboration, A. M. Sirunyan *et al.*, "Nuclear modification factor of D^0 mesons in PbPb collisions at $\sqrt{s_{NN}} = 5.02$ TeV," *Phys. Lett.* **B782** (2018) 474–496, `arXiv:1708.04962` `[nucl-ex]`.

[32] **ALICE** Collaboration, S. Acharya *et al.*, "Measurement of D^0, D^+, D^{*+} and D_s^+ production in Pb-Pb collisions at $\sqrt{s_{NN}} = 5.02$ TeV," *Submitted to: JHEP* (2018) , `arXiv:1804.09083` `[nucl-ex]`.

[33] J.-Y. Ollitrault, "Anisotropy as a signature of transverse collective flow," *Phys. Rev.* **D46** (1992) 229.

[34] S. Voloshin and Y. Zhang, "Flow study in relativistic nuclear collisions by Fourier expansion of Azimuthal particle distributions," *Z. Phys.* **C70** (1996) 665, `arXiv:hep-ph/9407282` `[hep-ph]`.

[35] A. M. Poskanzer and S. A. Voloshin, "Methods for analyzing anisotropic flow in relativistic nuclear collisions," *Phys. Rev.* **C58** (1998) 1671, `arXiv:nucl-ex/9805001` `[nucl-ex]`.

[36] G.-Y. Qin, H. Petersen, S. A. Bass, and B. Muller, "Translation of collision geometry fluctuations into momentum anisotropies in relativistic heavy-ion collisions," *Phys. Rev.* **C82** (2010) 064903, `arXiv:1009.1847` `[nucl-th]`.

[37] S. Batsouli, S. Kelly, M. Gyulassy, and J. L. Nagle, "Does the charm flow at RHIC?," *Phys. Lett.* **B557** (2003) 26, `arXiv:nucl-th/0212068` `[nucl-th]`.

[38] D. Molnar, "Charm elliptic flow from quark coalescence dynamics," *J. Phys.* **G31** (2005) S421, `arXiv:nucl-th/0410041` `[nucl-th]`.

[39] V. Greco, C. M. Ko, and R. Rapp, "Quark coalescence for charmed mesons in ultrarelativistic heavy ion collisions," *Phys. Lett.* **B595** (2004) 202, `arXiv:nucl-th/0312100` `[nucl-th]`.

[40] M. Gyulassy, I. Vitev, and X. N. Wang, "High p_T azimuthal asymmetry in noncentral A+A at RHIC," *Phys. Rev. Lett.* **86** (2001) 2537, `arXiv:nucl-th/0012092` `[nucl-th]`.

[41] E. V. Shuryak, "The Azimuthal asymmetry at large p_T seem to be too large for a 'jet quenching'," *Phys. Rev.* **C66** (2002) 027902, `arXiv:nucl-th/0112042` `[nucl-th]`.

[42] **STAR** Collaboration, L. Adamczyk *et al.*, "Elliptic flow of electrons from heavy-flavor hadron decays in Au+Au collisions at $\sqrt{s_{NN}} = 200$, 62.4, and 39 GeV," *Phys. Rev.* **C95** (2017) 034907,

arXiv:1405.6348 [hep-ex].

[43] **STAR** Collaboration, L. Adamczyk *et al.*, "Measurement of D^0 Azimuthal Anisotropy at Midrapidity in Au+Au Collisions at $\sqrt{s_{NN}}$=200 GeV," *Phys. Rev. Lett.* **118** no. 21, (2017) 212301, arXiv:1701.06060 [nucl-ex].

[44] **ALICE** Collaboration, B. Abelev *et al.*, "D meson elliptic flow in non-central Pb-Pb collisions at $\sqrt{s_{NN}} = 2.76$ TeV," *Phys. Rev. Lett.* **111** (2013) 102301, arXiv:1305.2707 [nucl-ex].

[45] **ALICE** Collaboration, B. Abelev *et al.*, "Azimuthal anisotropy of D meson production in Pb-Pb collisions at $\sqrt{s_{NN}} = 2.76$ TeV," *Phys. Rev.* **C90** (2014) 034904, arXiv:1405.2001 [nucl-ex].

[46] **ALICE** Collaboration, J. Adam *et al.*, "Elliptic flow of electrons from heavy-flavour hadron decays at mid-rapidity in Pb-Pb collisions at $\sqrt{s_{NN}} = 2.76$ TeV," *JHEP* **09** (2016) 028, arXiv:1606.00321 [nucl-ex].

[47] **ALICE** Collaboration, J. Adam *et al.*, "Elliptic flow of muons from heavy-flavour hadron decays at forward rapidity in Pb-Pb collisions at $\sqrt{s_{NN}} = 2.76$ TeV," *Phys. Lett.* **B753** (2016) 41, arXiv:1507.03134 [nucl-ex].

[48] **ALICE** Collaboration, S. Acharya *et al.*, "D-meson azimuthal anisotropy in midcentral Pb-Pb collisions at $\sqrt{\mathbf{s}_{NN}} = \mathbf{5.02}$ TeV," *Phys. Rev. Lett.* **120** no. 10, (2018) 102301, arXiv:1707.01005 [nucl-ex].

[49] **CMS** Collaboration, A. M. Sirunyan *et al.*, "Measurement of prompt D^0 meson azimuthal anisotropy in Pb-Pb collisions at $\sqrt{s_{NN}} = 5.02$ TeV," *Phys. Rev. Lett.* **120** no. 20, (2018) 202301, arXiv:1708.03497 [nucl-ex].

[50] J. Uphoff, O. Fochler, Z. Xu, and C. Greiner, "Open Heavy Flavor in Pb+Pb Collisions at $\sqrt{s} = 2.76$ TeV within a Transport Model," *Phys. Lett.* **B717** (2012) 430, arXiv:1205.4945 [hep-ph].

[51] M. He, R. J. Fries, and R. Rapp, "Heavy Flavor at the Large Hadron Collider in a Strong Coupling Approach," *Phys. Lett.* **B735** (2014) 445, arXiv:1401.3817 [nucl-th].

[52] M. Monteno, W. M. Alberico, A. Beraudo, A. De Pace, A. Molinari, M. Nardi, and F. Prino, "Heavy-flavor dynamics in nucleus-nucleus collisions: from RHIC to LHC," *J. Phys.* **G38** (2011) 124144, arXiv:1107.0256 [hep-ph].

[53] M. Djordjevic and M. Djordjevic, "Predictions of heavy-flavor suppression at 5.1 TeV Pb+Pb collisions at the CERN Large Hadron Collider," *Phys. Rev.* **C92** (2015) 024918, arXiv:1505.04316 [nucl-th].

[54] S. Cao, G.-Y. Qin, and S. A. Bass, "Heavy-quark dynamics and hadronization in ultrarelativistic heavy-ion collisions: Collisional versus radiative energy loss," *Phys. Rev.* **C88** (2013) 044907, arXiv:1308.0617 [nucl-th].

[55] T. Song, H. Berrehrah, D. Cabrera, W. Cassing, and E. Bratkovskaya, "Charm production in Pb + Pb collisions at energies available at the CERN Large Hadron Collider," *Phys. Rev.* **C93** (2016) 034906, arXiv:1512.00891 [nucl-th].

[56] M. Nahrgang, J. Aichelin, P. B. Gossiaux, and K. Werner, "Influence of hadronic bound states above T_c on heavy-quark observables in Pb + Pb collisions at at the CERN Large Hadron Collider," *Phys. Rev.* **C89** (2014) 014905, arXiv:1305.6544 [hep-ph].

[57] J. Uphoff, O. Fochler, Z. Xu, and C. Greiner, "Elastic and radiative heavy quark interactions in ultra-relativistic heavy-ion collisions," *J. Phys.* **G42** (2015) 115106, arXiv:1408.2964 [hep-ph].

[58] A. Beraudo, A. De Pace, M. Monteno, M. Nardi, and F. Prino, "Heavy flavors in heavy-ion collisions: quenching, flow and correlations," *Eur. Phys. J.* **C75** (2015) 121, arXiv:1410.6082 [hep-ph].

[59] S. Cao, T. Luo, G.-Y. Qin, and X.-N. Wang, "Heavy and light flavor jet quenching at RHIC and

LHC energies," *Phys. Lett.* **B777** (2018) 255–259, arXiv:1703.00822 [nucl-th].

[60] G. D. Moore and D. Teaney, "How much do heavy quarks thermalize in a heavy ion collision?," *Phys. Rev.* **C71** (2005) 064904, arXiv:hep-ph/0412346 [hep-ph].

[61] J. Schukraft, A. Timmins, and S. A. Voloshin, "Ultra-relativistic nuclear collisions: event shape engineering," *Phys. Lett.* **B719** (2013) 394–398, arXiv:1208.4563 [nucl-ex].

[62] **ALICE** Collaboration, J. Adam *et al.*, "Event shape engineering for inclusive spectra and elliptic flow in Pb-Pb collisions at $\sqrt{s_{\mathrm{NN}}} = 2.76$ TeV," *Phys. Rev.* **C93** no. 3, (2016) 034916, arXiv:1507.06194 [nucl-ex].

[63] **ATLAS** Collaboration, G. Aad *et al.*, "Measurement of the correlation between flow harmonics of different order in lead–lead collisions at $\sqrt{s_{\mathrm{NN}}}$=2.76 TeV with the ATLAS detector," *Phys. Rev.* **C92** no. 3, (2015) 034903, arXiv:1504.01289 [hep-ex].

[64] **ALICE** Collaboration, S. Acharya *et al.*, "Constraining the magnitude of the Chiral Magnetic Effect with Event Shape Engineering in Pb-Pb collisions at $\sqrt{s_{\mathrm{NN}}} = 2.76$ TeV," *Phys. Lett.* **B777** (2018) 151–162, arXiv:1709.04723 [nucl-ex].

[65] **CMS** Collaboration, A. M. Sirunyan *et al.*, "Constraints on the chiral magnetic effect using charge-dependent azimuthal correlations in pPb and PbPb collisions at the CERN Large Hadron Collider," *Phys. Rev.* **C97** no. 4, (2018) 044912, arXiv:1708.01602 [nucl-ex].

[66] **ALICE** Collaboration, B. Abelev *et al.*, "Anisotropic flow of charged hadrons, pions and (anti-)protons measured at high transverse momentum in Pb-Pb collisions at $\sqrt{s_{\mathrm{NN}}}$=2.76 TeV," *Phys. Lett.* **B719** (2013) 18–28, arXiv:1205.5761 [nucl-ex].

[67] U. Heinz and R. Snellings, "Collective flow and viscosity in relativistic heavy-ion collisions," *Ann. Rev. Nucl. Part. Sci.* **63** (2013) 123–151, arXiv:1301.2826 [nucl-th].

[68] F. G. Gardim, F. Grassi, M. Luzum, and J.-Y. Ollitrault, "Characterizing the hydrodynamic response to the initial conditions," *Nucl. Phys.* **A904-905** (2013) 503c–506c, arXiv:1210.8422 [nucl-th].

[69] S. A. Voloshin, A. M. Poskanzer, and R. Snellings, "Collective phenomena in non-central nuclear collisions," *Landolt-Bornstein* **23** (2010) 293–333, arXiv:0809.2949 [nucl-ex].

[70] W. Ke, Y. Xu, and S. A. Bass, "A linearized Boltzmann–Langevin model for heavy quark transport in hot and dense QCD matter," arXiv:1806.08848 [nucl-th].

[71] C. A. G. Prado, J. Noronha-Hostler, R. Katz, A. A. P. Suaide, J. Noronha, M. G. Munhoz, and M. R. Cosentino, "Event-by-event correlations between soft hadrons and D^0 mesons in 5.02 TeV PbPb collisions at the CERN Large Hadron Collider," *Phys. Rev.* **C96** no. 6, (2017) 064903, arXiv:1611.02965 [nucl-th].

[72] P. B. Gossiaux, J. Aichelin, M. Nahrgang, V. Ozvenchuk, and K. Werner, "Global view on coupled dynamics of heavy and light flavor observables from EPOSHQ," *Nucl. Phys.* **A967** (2017) 672–675, arXiv:1705.02271 [hep-ph].

[73] **ALICE** Collaboration, K. Aamodt *et al.*, "The ALICE experiment at the CERN LHC," *JINST* **3** (2008) S08002.

[74] **ALICE** Collaboration, B. Abelev *et al.*, "Performance of the ALICE Experiment at the CERN LHC," *Int. J. Mod. Phys.* **A29** (2014) 1430044, arXiv:1402.4476 [nucl-ex].

[75] R. J. Glauber and G. Matthiae, "High-energy scattering of protons by nuclei," *Nucl. Phys.* **B21** (1970) 135–157.

[76] M. L. Miller, K. Reygers, S. J. Sanders, and P. Steinberg, "Glauber modeling in high energy nuclear collisions," *Ann. Rev. Nucl. Part. Sci.* **57** (2007) 205–243, arXiv:nucl-ex/0701025 [nucl-ex].

[77] **ALICE** Collaboration, B. Abelev *et al.*, "Centrality determination of Pb-Pb collisions at $\sqrt{s_{NN}} = 2.76$ TeV with ALICE," *Phys. Rev.* **C88** no. 4, (2013) 044909, arXiv:1301.4361 [nucl-ex].

[78] **STAR** Collaboration, C. Adler *et al.*, "Elliptic flow from two and four particle correlations in Au+Au collisions at $\sqrt{s_{\mathrm{NN}}} = 130$ GeV," *Phys. Rev.* **C66** (2002) 034904, `arXiv:nucl-ex/0206001 [nucl-ex]`.

[79] I. Selyuzhenkov and S. Voloshin, "Effects of non-uniform acceptance in anisotropic flow measurement," *Phys. Rev.* **C77** (2008) 034904, `arXiv:0707.4672 [nucl-th]`.

[80] **Particle Data Group** Collaboration, C. Patrignani *et al.*, "Review of Particle Physics," *Chin. Phys.* **C40** no. 10, (2016) 100001.

[81] R. Brun, F. Carminati, and S. Giani, "CERN Program Library Long Write-up, W5013 GEANT Detector Description and Simulation Tool," Tech. Rep. CERN-W-5013, 1994.

[82] X.-N. Wang and M. Gyulassy, "HIJING: A Monte Carlo model for multiple jet production in pp, pA and AA collisions," *Phys. Rev.* **D44** (1991) 3501–3516.

[83] T. Sjostrand, S. Mrenna, and P. Z. Skands, "PYTHIA 6.4 Physics and Manual," *JHEP* **05** (2006) 026, `arXiv:hep-ph/0603175 [hep-ph]`.

[84] P. Z. Skands, "Tuning Monte Carlo Generators: The Perugia Tunes," *Phys. Rev.* **D82** (2010) 074018, `arXiv:1005.3457 [hep-ph]`.

[85] M. Cacciari, M. Greco, and P. Nason, "The p_{T} spectrum in heavy flavor hadroproduction," *JHEP* **05** (1998) 007, `arXiv:hep-ph/9803400 [hep-ph]`.

[86] M. Cacciari, S. Frixione, and P. Nason, "The p_{T} spectrum in heavy flavor photoproduction," *JHEP* **03** (2001) 006, `arXiv:hep-ph/0102134 [hep-ph]`.

[87] D. J. Lange, "The EvtGen particle decay simulation package," *Nucl. Instrum. Meth.* **A462** (2001) 152–155.

[88] **ALICE** Collaboration, J. Adam *et al.*, "Centrality dependence of high-p_T D meson suppression in Pb-Pb collisions at $\sqrt{s_{\mathrm{NN}}} = 2.76$ TeV," *JHEP* **11** (2015) 205, `arXiv:1506.06604 [nucl-ex]`. [Addendum: JHEP06,032(2017)].

[89] J. Aichelin, P. B. Gossiaux, and T. Gousset, "Radiative and Collisional Energy Loss of Heavy Quarks in Deconfined Matter," *Acta Phys. Polon.* **B43** (2012) 655–662, `arXiv:1201.4192 [nucl-th]`.

[90] V. Greco, H. van Hees, and R. Rapp, "Heavy-quark kinetics at RHIC and LHC," in *Nuclear physics. Proceedings, 23rd International Conference, INPC 2007, Tokyo, Japan, June 3-8, 2007.* 2007. `arXiv:0709.4452 [hep-ph]`.

[91] **ALICE** Collaboration, S. Acharya *et al.*, "Anisotropic flow of identified particles in Pb-Pb collisions at $\sqrt{s_{\mathrm{NN}}} = 5.02$ TeV," `arXiv:1805.04390 [nucl-ex]`.

[92] **ALICE** Collaboration, B. Abelev *et al.*, "Elliptic flow of identified hadrons in Pb-Pb collisions at $\sqrt{s_{\mathrm{NN}}} = 2.76$ TeV," *JHEP* **06** (2015) 190, `arXiv:1405.4632 [nucl-ex]`.

[93] **ALICE** Collaboration, B. Abelev *et al.*, "Technical Design Report for the Upgrade of the ALICE Inner Tracking System," *J. Phys.* **G41** (2014) 087002.

[94] **ALICE** Collaboration, B. Abelev *et al.*, "Upgrade of the ALICE Experiment: Letter Of Intent," *J. Phys.* **G41** (2014) 087001.

A   The ALICE Collaboration

S. Acharya[139], F.T.-. Acosta[20], D. Adamová[93], A. Adler[74], J. Adolfsson[80], M.M. Aggarwal[98], G. Aglieri
Rinella[34], M. Agnello[31], N. Agrawal[48], Z. Ahammed[139], S.U. Ahn[76], S. Aiola[144], A. Akindinov[64],
M. Al-Turany[104], S.N. Alam[139], D.S.D. Albuquerque[121], D. Aleksandrov[87], B. Alessandro[58], H.M. Alfanda[6],
R. Alfaro Molina[72], Y. Ali[15], A. Alici[10,27,53], A. Alkin[2], J. Alme[22], T. Alt[69], L. Altenkamper[22], I. Altsybeev[111],
M.N. Anaam[6], C. Andrei[47], D. Andreou[34], H.A. Andrews[108], A. Andronic[104,142], M. Angeletti[34],
V. Anguelov[102], C. Anson[16], T. Antičić[105], F. Antinori[56], P. Antonioli[53], R. Anwar[125], N. Apadula[79],
L. Aphecetche[113], H. Appelshäuser[69], S. Arcelli[27], R. Arnaldi[58], M. Arratia[79], I.C. Arsene[21], M. Arslandok[102],
A. Augustinus[34], R. Averbeck[104], M.D. Azmi[17], A. Badalà[55], Y.W. Baek[40,60], S. Bagnasco[58], R. Bailhache[69],
R. Bala[99], A. Baldisseri[135], M. Ball[42], R.C. Baral[85], R. Barbera[28], F. Barile[52], L. Barioglio[26], G.G. Barnaföldi[143],
L.S. Barnby[92], V. Barret[132], P. Bartalini[6], K. Barth[34], E. Bartsch[69], N. Bastid[132], S. Basu[141], G. Batigne[113],
B. Batyunya[75], P.C. Batzing[21], J.L. Bazo Alba[109], I.G. Bearden[88], H. Beck[102], C. Bedda[63], N.K. Behera[60],
I. Belikov[134], F. Bellini[34], H. Bello Martinez[44], R. Bellwied[125], L.G.E. Beltran[119], V. Belyaev[91], G. Bencedi[143],
S. Beole[26], A. Bercuci[47], Y. Berdnikov[96], D. Berenyi[143], R.A. Bertens[128], D. Berzano[34,58], L. Betev[34],
P.P. Bhaduri[139], A. Bhasin[99], I.R. Bhat[99], H. Bhatt[48], B. Bhattacharjee[41], J. Bhom[117], A. Bianchi[26],
L. Bianchi[26,125], N. Bianchi[51], J. Bielčík[37], J. Bielčíková[93], A. Bilandzic[103,116], G. Biro[143], R. Biswas[3],
S. Biswas[3], J.T. Blair[118], D. Blau[87], C. Blume[69], G. Boca[137], F. Bock[34], A. Bogdanov[91], L. Boldizsár[143],
A. Bolozdynya[91], M. Bombara[38], G. Bonomi[138], M. Bonora[34], H. Borel[135], A. Borissov[102,142], M. Borri[127],
E. Botta[26], C. Bourjau[88], L. Bratrud[69], P. Braun-Munzinger[104], M. Bregant[120], T.A. Broker[69], M. Broz[37],
E.J. Brucken[43], E. Bruna[58], G.E. Bruno[33], D. Budnikov[106], H. Buesching[69], S. Bufalino[31], P. Buhler[112],
P. Buncic[34], O. Busch[I,131], Z. Buthelezi[73], J.B. Butt[15], J.T. Buxton[95], J. Cabala[115], D. Caffarri[89], H. Caines[144],
A. Caliva[104], E. Calvo Villar[109], R.S. Camacho[44], P. Camerini[25], A.A. Capon[112], W. Carena[34],
F. Carnesecchi[10,27], J. Castillo Castellanos[135], A.J. Castro[128], E.A.R. Casula[54], C. Ceballos Sanchez[8],
S. Chandra[139], B. Chang[126], W. Chang[6], S. Chapeland[34], M. Chartier[127], S. Chattopadhyay[139],
S. Chattopadhyay[107], A. Chauvin[24], C. Cheshkov[133], B. Cheynis[133], V. Chibante Barroso[34], D.D. Chinellato[121],
S. Cho[60], P. Chochula[34], T. Chowdhury[132], P. Christakoglou[89], C.H. Christensen[88], P. Christiansen[80], T. Chujo[131],
S.U. Chung[18], C. Cicalo[54], L. Cifarelli[10,27], F. Cindolo[53], J. Cleymans[124], F. Colamaria[52], D. Colella[52],
A. Collu[79], M. Colocci[27], M. Concas[II,58], G. Conesa Balbastre[78], Z. Conesa del Valle[61], J.G. Contreras[37],
T.M. Cormier[94], Y. Corrales Morales[58], P. Cortese[32], M.R. Cosentino[122], F. Costa[34], S. Costanza[137],
J. Crkovská[61], P. Crochet[132], E. Cuautle[70], L. Cunqueiro[94,142], D. Dabrowski[140], T. Dahms[103,116], A. Dainese[56],
F.P.A. Damas[113,135], S. Dani[66], M.C. Danisch[102], A. Danu[68], D. Das[107], I. Das[107], S. Das[3], A. Dash[85], S. Dash[48],
S. De[49], A. De Caro[30], G. de Cataldo[52], C. de Conti[120], J. de Cuveland[39], A. De Falco[24], D. De Gruttola[10,30],
N. De Marco[58], S. De Pasquale[30], R.D. De Souza[121], H.F. Degenhardt[120], A. Deisting[102,104], A. Deloff[84],
S. Delsanto[26], C. Deplano[89], P. Dhankher[48], D. Di Bari[33], A. Di Mauro[34], R.A. Diaz[8], T. Dietel[124],
P. Dillenseger[69], Y. Ding[6], R. Divià[34], Ø. Djuvsland[22], A. Dobrin[34], D. Domenicis Gimenez[120], B. Dönigus[69],
O. Dordic[21], A.K. Dubey[139], A. Dubla[104], L. Ducroux[133], S. Dudi[98], A.K. Duggal[98], M. Dukhishyam[85],
P. Dupieux[132], R.J. Ehlers[144], D. Elia[52], H. Engel[74], E. Epple[144], B. Erazmus[113], F. Erhardt[97], A. Erokhin[111],
M.R. Ersdal[22], B. Espagnon[61], G. Eulisse[34], J. Eum[18], D. Evans[108], S. Evdokimov[90], L. Fabbietti[103,116],
M. Faggin[29], J. Faivre[78], A. Fantoni[51], M. Fasel[94], L. Feldkamp[142], A. Feliciello[58], G. Feofilov[111], A. Fernández
Téllez[44], A. Ferretti[26], A. Festanti[34], V.J.G. Feuillard[102], J. Figiel[117], M.A.S. Figueredo[120], S. Filchagin[106],
D. Finogeev[62], F.M. Fionda[22], G. Fiorenza[52], F. Flor[125], M. Floris[34], S. Foertsch[73], P. Foka[104], S. Fokin[87],
E. Fragiacomo[59], A. Francescon[34], A. Francisco[113], U. Frankenfeld[104], G.G. Fronze[26], U. Fuchs[34], C. Furget[78],
A. Furs[62], M. Fusco Girard[30], J.J. Gaardhøje[88], M. Gagliardi[26], A.M. Gago[109], K. Gajdosova[88], M. Gallio[26],
C.D. Galvan[119], P. Ganoti[83], C. Garabatos[104], E. Garcia-Solis[11], K. Garg[28], C. Gargiulo[34], K. Garner[142],
P. Gasik[103,116], E.F. Gauger[118], M.B. Gay Ducati[71], M. Germain[113], J. Ghosh[107], P. Ghosh[139], S.K. Ghosh[3],
P. Gianotti[51], P. Giubellino[58,104], P. Giubilato[29], P. Glässel[102], D.M. Gómez Coral[72], A. Gomez Ramirez[74],
V. Gonzalez[104], P. González-Zamora[44], S. Gorbunov[39], L. Görlich[117], S. Gotovac[35], V. Grabski[72],
L.K. Graczykowski[140], K.L. Graham[108], L. Greiner[79], A. Grelli[63], C. Grigoras[34], V. Grigoriev[91], A. Grigoryan[1],
S. Grigoryan[75], J.M. Gronefeld[104], F. Grosa[31], J.F. Grosse-Oetringhaus[34], R. Grosso[104], R. Guernane[78],
B. Guerzoni[27], M. Guittiere[113], K. Gulbrandsen[88], T. Gunji[130], A. Gupta[99], R. Gupta[99], I.B. Guzman[44],
R. Haake[34,144], M.K. Habib[104], C. Hadjidakis[61], H. Hamagaki[81], G. Hamar[143], M. Hamid[6], J.C. Hamon[134],
R. Hannigan[118], M.R. Haque[63], A. Harlenderova[104], J.W. Harris[144], A. Harton[11], H. Hassan[78],
D. Hatzifotiadou[10,53], P. Hauer[42], S. Hayashi[130], S.T. Heckel[69], E. Hellbär[69], H. Helstrup[36], A. Herghelegiu[47],
E.G. Hernandez[44], G. Herrera Corral[9], F. Herrmann[142], K.F. Hetland[36], T.E. Hilden[43], H. Hillemanns[34],
C. Hills[127], B. Hippolyte[134], B. Hohlweger[103], D. Horak[37], S. Hornung[104], R. Hosokawa[78,131], J. Hota[66],
P. Hristov[34], C. Huang[61], C. Hughes[128], P. Huhn[69], T.J. Humanic[95], H. Hushnud[107], N. Hussain[41], T. Hussain[17],

D. Hutter[39], D.S. Hwang[19], J.P. Iddon[127], R. Ilkaev[106], M. Inaba[131], M. Ippolitov[87], M.S. Islam[107], M. Ivanov[104], V. Ivanov[96], V. Izucheev[90], B. Jacak[79], N. Jacazio[27], P.M. Jacobs[79], M.B. Jadhav[48], S. Jadlovska[115], J. Jadlovsky[115], S. Jaelani[63], C. Jahnke[116,120], M.J. Jakubowska[140], M.A. Janik[140], C. Jena[85], M. Jercic[97], O. Jevons[108], R.T. Jimenez Bustamante[104], M. Jin[125], P.G. Jones[108], A. Jusko[108], P. Kalinak[65], A. Kalweit[34], J.H. Kang[145], V. Kaplin[91], S. Kar[6], A. Karasu Uysal[77], O. Karavichev[62], T. Karavicheva[62], P. Karczmarczyk[34], E. Karpechev[62], U. Kebschull[74], R. Keidel[46], D.L.D. Keijdener[63], M. Keil[34], B. Ketzer[42], Z. Khabanova[89], A.M. Khan[6], S. Khan[17], S.A. Khan[139], A. Khanzadeev[96], Y. Kharlov[90], A. Khatun[17], A. Khuntia[49], M.M. Kielbowicz[117], B. Kileng[36], B. Kim[60], B. Kim[131], D. Kim[145], D.J. Kim[126], E.J. Kim[13], H. Kim[145], J.S. Kim[40], J. Kim[102], J. Kim[13], M. Kim[60,102], S. Kim[19], T. Kim[145], T. Kim[145], K. Kindra[98], S. Kirsch[39], I. Kisel[39], S. Kiselev[64], A. Kisiel[140], J.L. Klay[5], C. Klein[69], J. Klein[58], C. Klein-Bösing[142], S. Klewin[102], A. Kluge[34], M.L. Knichel[34], A.G. Knospe[125], C. Kobdaj[114], M. Kofarago[143], M.K. Köhler[102], T. Kollegger[104], N. Kondratyeva[91], E. Kondratyuk[90], A. Konevskikh[62], P.J. Konopka[34], M. Konyushikhin[141], L. Koska[115], O. Kovalenko[84], V. Kovalenko[111], M. Kowalski[117], I. Králik[65], A. Kravčáková[38], L. Kreis[104], M. Krivda[65,108], F. Krizek[93], M. Krüger[69], E. Kryshen[96], M. Krzewicki[39], A.M. Kubera[95], V. Kučera[60,93], C. Kuhn[134], P.G. Kuijer[89], J. Kumar[48], L. Kumar[98], S. Kumar[48], S. Kundu[85], P. Kurashvili[84], A. Kurepin[62], A.B. Kurepin[62], S. Kushpil[93], J. Kvapil[108], M.J. Kweon[60], Y. Kwon[145], S.L. La Pointe[39], P. La Rocca[28], Y.S. Lai[79], I. Lakomov[34], R. Langoy[123], K. Lapidus[34,144], A. Lardeux[21], P. Larionov[51], E. Laudi[34], R. Lavicka[37], R. Lea[25], L. Leardini[102], S. Lee[145], F. Lehas[89], S. Lehner[112], J. Lehrbach[39], R.C. Lemmon[92], I. León Monzón[119], P. Lévai[143], X. Li[12], X.L. Li[6], J. Lien[123], R. Lietava[108], B. Lim[18], S. Lindal[21], V. Lindenstruth[39], S.W. Lindsay[127], C. Lippmann[104], M.A. Lisa[95], V. Litichevskyi[43], A. Liu[79], H.M. Ljunggren[80], W.J. Llope[141], D.F. Lodato[63], V. Loginov[91], C. Loizides[79,94], P. Loncar[35], X. Lopez[132], E. López Torres[8], P. Luettig[69], J.R. Luhder[142], M. Lunardon[29], G. Luparello[59], M. Lupi[34], A. Maevskaya[62], M. Mager[34], S.M. Mahmood[21], A. Maire[134], R.D. Majka[144], M. Malaev[96], Q.W. Malik[21], L. Malinina[III,75], D. Mal'Kevich[64], P. Malzacher[104], A. Mamonov[106], V. Manko[87], F. Manso[132], V. Manzari[52], Y. Mao[6], M. Marchisone[133], J. Mareš[67], G.V. Margagliotti[25], A. Margotti[53], J. Margutti[63], A. Marín[104], C. Markert[118], M. Marquard[69], N.A. Martin[102,104], P. Martinengo[34], J.L. Martinez[125], M.I. Martínez[44], G. Martínez García[113], M. Martinez Pedreira[34], S. Masciocchi[104], M. Masera[26], A. Masoni[54], L. Massacrier[61], E. Masson[113], A. Mastroserio[52,136], A.M. Mathis[103,116], P.F.T. Matuoka[120], A. Matyja[117,128], C. Mayer[117], M. Mazzilli[33], M.A. Mazzoni[57], F. Meddi[23], Y. Melikyan[91], A. Menchaca-Rocha[72], E. Meninno[30], M. Meres[14], S. Mhlanga[124], Y. Miake[131], L. Micheletti[26], M.M. Mieskolainen[43], D.L. Mihaylov[103], K. Mikhaylov[64,75], A. Mischke[63], A.N. Mishra[70], D. Miśkowiec[104], J. Mitra[139], C.M. Mitu[68], N. Mohammadi[34], A.P. Mohanty[63], B. Mohanty[85], M. Mohisin Khan[IV,17], D.A. Moreira De Godoy[142], L.A.P. Moreno[44], S. Moretto[29], A. Morreale[113], A. Morsch[34], T. Mrnjavac[34], V. Muccifora[51], E. Mudnic[35], D. Mühlheim[142], S. Muhuri[139], M. Mukherjee[3], J.D. Mulligan[144], M.G. Munhoz[120], K. Münning[42], R.H. Munzer[69], H. Murakami[130], S. Murray[73], L. Musa[34], J. Musinsky[65], C.J. Myers[125], J.W. Myrcha[140], B. Naik[48], R. Nair[84], B.K. Nandi[48], R. Nania[10,53], E. Nappi[52], A. Narayan[48], M.U. Naru[15], A.F. Nassirpour[80], H. Natal da Luz[120], C. Nattrass[128], S.R. Navarro[44], K. Nayak[85], R. Nayak[48], T.K. Nayak[85,139], S. Nazarenko[106], R.A. Negrao De Oliveira[34,69], L. Nellen[70], S.V. Nesbo[36], G. Neskovic[39], F. Ng[125], J. Niedziela[34,140], B.S. Nielsen[88], S. Nikolaev[87], S. Nikulin[87], V. Nikulin[96], F. Noferini[10,53], P. Nomokonov[75], G. Nooren[63], J.C.C. Noris[44], J. Norman[78], A. Nyanin[87], J. Nystrand[22], M. Ogino[81], H. Oh[145], A. Ohlson[102], J. Oleniacz[140], A.C. Oliveira Da Silva[120], M.H. Oliver[144], J. Onderwaater[104], C. Oppedisano[58], R. Orava[43], M. Oravec[115], A. Ortiz Velasquez[70], A. Oskarsson[80], J. Otwinowski[117], K. Oyama[81], Y. Pachmayer[102], V. Pacik[88], D. Pagano[138], G. Paić[70], P. Palni[6], J. Pan[141], A.K. Pandey[48], S. Panebianco[135], V. Papikyan[1], P. Pareek[49], J. Park[60], J.E. Parkkila[126], S. Parmar[98], A. Passfeld[142], S.P. Pathak[125], R.N. Patra[139], B. Paul[58], H. Pei[6], T. Peitzmann[63], X. Peng[6], L.G. Pereira[71], H. Pereira Da Costa[135], D. Peresunko[87], E. Perez Lezama[69], V. Peskov[69], Y. Pestov[4], V. Petráček[37], M. Petrovici[47], C. Petta[28], R.P. Pezzi[71], S. Piano[59], M. Pikna[14], P. Pillot[113], L.O.D.L. Pimentel[88], O. Pinazza[34,53], L. Pinsky[125], S. Pisano[51], D.B. Piyarathna[125], M. Płoskoń[79], M. Planinic[97], F. Pliquett[69], J. Pluta[140], S. Pochybova[143], P.L.M. Podesta-Lerma[119], M.G. Poghosyan[94], B. Polichtchouk[90], N. Poljak[97], W. Poonsawat[114], A. Pop[47], H. Poppenborg[142], S. Porteboeuf-Houssais[132], V. Pozdniakov[75], S.K. Prasad[3], R. Preghenella[53], F. Prino[58], C.A. Pruneau[141], I. Pshenichnov[62], M. Puccio[26], V. Punin[106], K. Puranapanda[139], J. Putschke[141], R.E. Quishpe[125], S. Raha[3], S. Rajput[99], J. Rak[126], A. Rakotozafindrabe[135], L. Ramello[32], F. Rami[134], R. Raniwala[100], S. Raniwala[100], S.S. Räsänen[43], B.T. Rascanu[69], R. Rath[49], V. Ratza[42], I. Ravasenga[31], K.F. Read[94,128], K. Redlich[V,84], A. Rehman[22], P. Reichelt[69], F. Reidt[34], X. Ren[6], R. Renfordt[69], A. Reshetin[62], J.-P. Revol[10], K. Reygers[102], V. Riabov[96], T. Richert[80,88], M. Richter[21], P. Riedler[34], W. Riegler[34], F. Riggi[28], C. Ristea[68], S.P. Rode[49], M. Rodríguez Cahuantzi[44], K. Røed[21], R. Rogalev[90], E. Rogochaya[75], D. Rohr[34], D. Röhrich[22], P.S. Rokita[140], F. Ronchetti[51], E.D. Rosas[70], K. Roslon[140], P. Rosnet[132], A. Rossi[29,56], A. Rotondi[137], F. Roukoutakis[83], C. Roy[134], P. Roy[107], O.V. Rueda[70], R. Rui[25], B. Rumyantsev[75],

26

A. Rustamov[86], E. Ryabinkin[87], Y. Ryabov[96], A. Rybicki[117], S. Saarinen[43], S. Sadhu[139], S. Sadovsky[90], K. Šafařík[34], S.K. Saha[139], B. Sahoo[48], P. Sahoo[49], R. Sahoo[49], S. Sahoo[66], P.K. Sahu[66], J. Saini[139], S. Sakai[131], M.A. Saleh[141], S. Sambyal[99], V. Samsonov[91,96], A. Sandoval[72], A. Sarkar[73], D. Sarkar[139], N. Sarkar[139], P. Sarma[41], M.H.P. Sas[63], E. Scapparone[53], F. Scarlassara[29], B. Schaefer[94], H.S. Scheid[69], C. Schiaua[47], R. Schicker[102], C. Schmidt[104], H.R. Schmidt[101], M.O. Schmidt[102], M. Schmidt[101], N.V. Schmidt[69,94], J. Schukraft[34], Y. Schutz[34,134], K. Schwarz[104], K. Schweda[104], G. Scioli[27], E. Scomparin[58], M. Šefčík[38], J.E. Seger[16], Y. Sekiguchi[130], D. Sekihata[45], I. Selyuzhenkov[91,104], S. Senyukov[134], E. Serradilla[72], P. Sett[48], A. Sevcenco[68], A. Shabanov[62], A. Shabetai[113], R. Shahoyan[34], W. Shaikh[107], A. Shangaraev[90], A. Sharma[98], A. Sharma[99], M. Sharma[99], N. Sharma[98], A.I. Sheikh[139], K. Shigaki[45], M. Shimomura[82], S. Shirinkin[64], Q. Shou[6,110], Y. Sibiriak[87], S. Siddhanta[54], T. Siemiarczuk[84], D. Silvermyr[80], G. Simatovic[89], G. Simonetti[34,103], R. Singaraju[139], R. Singh[85], R. Singh[99], V. Singhal[139], T. Sinha[107], B. Sitar[14], M. Sitta[32], T.B. Skaali[21], M. Slupecki[126], N. Smirnov[144], R.J.M. Snellings[63], T.W. Snellman[126], J. Sochan[115], C. Soncco[109], J. Song[18,60], A. Songmoolnak[114], F. Soramel[29], S. Sorensen[128], F. Sozzi[104], I. Sputowska[117], J. Stachel[102], I. Stan[68], P. Stankus[94], E. Stenlund[80], D. Stocco[113], M.M. Storetvedt[36], P. Strmen[14], A.A.P. Suaide[120], T. Sugitate[45], C. Suire[61], M. Suleymanov[15], M. Suljic[34], R. Sultanov[64], M. Šumbera[93], S. Sumowidagdo[50], K. Suzuki[112], S. Swain[66], A. Szabo[14], I. Szarka[14], U. Tabassam[15], J. Takahashi[121], G.J. Tambave[22], N. Tanaka[131], M. Tarhini[113], M.G. Tarzila[47], A. Tauro[34], G. Tejeda Muñoz[44], A. Telesca[34], C. Terrevoli[29], B. Teyssier[133], D. Thakur[49], S. Thakur[139], D. Thomas[118], F. Thoresen[88], R. Tieulent[133], A. Tikhonov[62], A.R. Timmins[125], A. Toia[69], N. Topilskaya[62], M. Toppi[51], S.R. Torres[119], S. Tripathy[49], S. Trogolo[26], G. Trombetta[33], L. Tropp[38], V. Trubnikov[2], W.H. Trzaska[126], T.P. Trzcinski[140], B.A. Trzeciak[63], T. Tsuji[130], A. Tumkin[106], R. Turrisi[56], T.S. Tveter[21], K. Ullaland[22], E.N. Umaka[125], A. Uras[133], G.L. Usai[24], A. Utrobicic[97], M. Vala[115], L. Valencia Palomo[44], N. Valle[137], N. van der Kolk[63], L.V.R. van Doremalen[63], J.W. Van Hoorne[34], M. van Leeuwen[63], P. Vande Vyvre[34], D. Varga[143], A. Vargas[44], M. Vargyas[126], R. Varma[48], M. Vasileiou[83], A. Vasiliev[87], O. Vázquez Doce[103,116], V. Vechernin[111], A.M. Veen[63], E. Vercellin[26], S. Vergara Limón[44], L. Vermunt[63], R. Vernet[7], R. Vértesi[143], L. Vickovic[35], J. Viinikainen[126], Z. Vilakazi[129], O. Villalobos Baillie[108], A. Villatoro Tello[44], G. Vino[52], A. Vinogradov[87], T. Virgili[30], V. Vislavicius[80,88], A. Vodopyanov[75], B. Volkel[34], M.A. Völkl[101], K. Voloshin[64], S.A. Voloshin[141], G. Volpe[33], B. von Haller[34], I. Vorobyev[103,116], D. Voscek[115], J. Vrláková[38], B. Wagner[22], M. Wang[6], Y. Watanabe[131], M. Weber[112], S.G. Weber[104], A. Wegrzynek[34], D.F. Weiser[102], S.C. Wenzel[34], J.P. Wessels[142], U. Westerhoff[142], A.M. Whitehead[124], E. Widmann[112], J. Wiechula[69], J. Wikne[21], G. Wilk[84], J. Wilkinson[53], G.A. Willems[34,142], E. Willsher[108], B. Windelband[102], W.E. Witt[128], R. Xu[6], S. Yalcin[77], K. Yamakawa[45], S. Yano[45,135], Z. Yin[6], H. Yokoyama[78,131], I.-K. Yoo[18], J.H. Yoon[60], S. Yuan[22], V. Yurchenko[2], V. Zaccolo[58], A. Zaman[15], C. Zampolli[34], H.J.C. Zanoli[120], N. Zardoshti[108], A. Zarochentsev[111], P. Závada[67], N. Zaviyalov[106], H. Zbroszczyk[140], M. Zhalov[96], X. Zhang[6], Y. Zhang[6], Z. Zhang[6,132], C. Zhao[21], V. Zherebchevskii[111], N. Zhigareva[64], D. Zhou[6], Y. Zhou[88], Z. Zhou[22], H. Zhu[6], J. Zhu[6], Y. Zhu[6], A. Zichichi[10,27], M.B. Zimmermann[34], G. Zinovjev[2]

Affiliation Notes

[I] Deceased
[II] Also at: Dipartimento DET del Politecnico di Torino, Turin, Italy
[III] Also at: M.V. Lomonosov Moscow State University, D.V. Skobeltsyn Institute of Nuclear, Physics, Moscow, Russia
[IV] Also at: Department of Applied Physics, Aligarh Muslim University, Aligarh, India
[V] Also at: Institute of Theoretical Physics, University of Wroclaw, Poland

Collaboration Institutes

[1] A.I. Alikhanyan National Science Laboratory (Yerevan Physics Institute) Foundation, Yerevan, Armenia
[2] Bogolyubov Institute for Theoretical Physics, National Academy of Sciences of Ukraine, Kiev, Ukraine
[3] Bose Institute, Department of Physics and Centre for Astroparticle Physics and Space Science (CAPSS), Kolkata, India
[4] Budker Institute for Nuclear Physics, Novosibirsk, Russia
[5] California Polytechnic State University, San Luis Obispo, California, United States

[6] Central China Normal University, Wuhan, China

[7] Centre de Calcul de l'IN2P3, Villeurbanne, Lyon, France

[8] Centro de Aplicaciones Tecnológicas y Desarrollo Nuclear (CEADEN), Havana, Cuba

[9] Centro de Investigación y de Estudios Avanzados (CINVESTAV), Mexico City and Mérida, Mexico

[10] Centro Fermi - Museo Storico della Fisica e Centro Studi e Ricerche "Enrico Fermi', Rome, Italy

[11] Chicago State University, Chicago, Illinois, United States

[12] China Institute of Atomic Energy, Beijing, China

[13] Chonbuk National University, Jeonju, Republic of Korea

[14] Comenius University Bratislava, Faculty of Mathematics, Physics and Informatics, Bratislava, Slovakia

[15] COMSATS Institute of Information Technology (CIIT), Islamabad, Pakistan

[16] Creighton University, Omaha, Nebraska, United States

[17] Department of Physics, Aligarh Muslim University, Aligarh, India

[18] Department of Physics, Pusan National University, Pusan, Republic of Korea

[19] Department of Physics, Sejong University, Seoul, Republic of Korea

[20] Department of Physics, University of California, Berkeley, California, United States

[21] Department of Physics, University of Oslo, Oslo, Norway

[22] Department of Physics and Technology, University of Bergen, Bergen, Norway

[23] Dipartimento di Fisica dell'Università 'La Sapienza' and Sezione INFN, Rome, Italy

[24] Dipartimento di Fisica dell'Università and Sezione INFN, Cagliari, Italy

[25] Dipartimento di Fisica dell'Università and Sezione INFN, Trieste, Italy

[26] Dipartimento di Fisica dell'Università and Sezione INFN, Turin, Italy

[27] Dipartimento di Fisica e Astronomia dell'Università and Sezione INFN, Bologna, Italy

[28] Dipartimento di Fisica e Astronomia dell'Università and Sezione INFN, Catania, Italy

[29] Dipartimento di Fisica e Astronomia dell'Università and Sezione INFN, Padova, Italy

[30] Dipartimento di Fisica 'E.R. Caianiello' dell'Università and Gruppo Collegato INFN, Salerno, Italy

[31] Dipartimento DISAT del Politecnico and Sezione INFN, Turin, Italy

[32] Dipartimento di Scienze e Innovazione Tecnologica dell'Università del Piemonte Orientale and INFN Sezione di Torino, Alessandria, Italy

[33] Dipartimento Interateneo di Fisica 'M. Merlin' and Sezione INFN, Bari, Italy

[34] European Organization for Nuclear Research (CERN), Geneva, Switzerland

[35] Faculty of Electrical Engineering, Mechanical Engineering and Naval Architecture, University of Split, Split, Croatia

[36] Faculty of Engineering and Science, Western Norway University of Applied Sciences, Bergen, Norway

[37] Faculty of Nuclear Sciences and Physical Engineering, Czech Technical University in Prague, Prague, Czech Republic

[38] Faculty of Science, P.J. Šafárik University, Košice, Slovakia

[39] Frankfurt Institute for Advanced Studies, Johann Wolfgang Goethe-Universität Frankfurt, Frankfurt, Germany

[40] Gangneung-Wonju National University, Gangneung, Republic of Korea

[41] Gauhati University, Department of Physics, Guwahati, India

[42] Helmholtz-Institut für Strahlen- und Kernphysik, Rheinische Friedrich-Wilhelms-Universität Bonn, Bonn, Germany

[43] Helsinki Institute of Physics (HIP), Helsinki, Finland

[44] High Energy Physics Group, Universidad Autónoma de Puebla, Puebla, Mexico

[45] Hiroshima University, Hiroshima, Japan

[46] Hochschule Worms, Zentrum für Technologietransfer und Telekommunikation (ZTT), Worms, Germany

[47] Horia Hulubei National Institute of Physics and Nuclear Engineering, Bucharest, Romania

[48] Indian Institute of Technology Bombay (IIT), Mumbai, India

[49] Indian Institute of Technology Indore, Indore, India

[50] Indonesian Institute of Sciences, Jakarta, Indonesia

[51] INFN, Laboratori Nazionali di Frascati, Frascati, Italy

[52] INFN, Sezione di Bari, Bari, Italy

[53] INFN, Sezione di Bologna, Bologna, Italy

[54] INFN, Sezione di Cagliari, Cagliari, Italy

[55] INFN, Sezione di Catania, Catania, Italy

[56] INFN, Sezione di Padova, Padova, Italy

[57] INFN, Sezione di Roma, Rome, Italy

[58] INFN, Sezione di Torino, Turin, Italy
[59] INFN, Sezione di Trieste, Trieste, Italy
[60] Inha University, Incheon, Republic of Korea
[61] Institut de Physique Nucléaire d'Orsay (IPNO), Institut National de Physique Nucléaire et de Physique des Particules (IN2P3/CNRS), Université de Paris-Sud, Université Paris-Saclay, Orsay, France
[62] Institute for Nuclear Research, Academy of Sciences, Moscow, Russia
[63] Institute for Subatomic Physics, Utrecht University/Nikhef, Utrecht, Netherlands
[64] Institute for Theoretical and Experimental Physics, Moscow, Russia
[65] Institute of Experimental Physics, Slovak Academy of Sciences, Košice, Slovakia
[66] Institute of Physics, Homi Bhabha National Institute, Bhubaneswar, India
[67] Institute of Physics of the Czech Academy of Sciences, Prague, Czech Republic
[68] Institute of Space Science (ISS), Bucharest, Romania
[69] Institut für Kernphysik, Johann Wolfgang Goethe-Universität Frankfurt, Frankfurt, Germany
[70] Instituto de Ciencias Nucleares, Universidad Nacional Autónoma de México, Mexico City, Mexico
[71] Instituto de Física, Universidade Federal do Rio Grande do Sul (UFRGS), Porto Alegre, Brazil
[72] Instituto de Física, Universidad Nacional Autónoma de México, Mexico City, Mexico
[73] iThemba LABS, National Research Foundation, Somerset West, South Africa
[74] Johann-Wolfgang-Goethe Universität Frankfurt Institut für Informatik, Fachbereich Informatik und Mathematik, Frankfurt, Germany
[75] Joint Institute for Nuclear Research (JINR), Dubna, Russia
[76] Korea Institute of Science and Technology Information, Daejeon, Republic of Korea
[77] KTO Karatay University, Konya, Turkey
[78] Laboratoire de Physique Subatomique et de Cosmologie, Université Grenoble-Alpes, CNRS-IN2P3, Grenoble, France
[79] Lawrence Berkeley National Laboratory, Berkeley, California, United States
[80] Lund University Department of Physics, Division of Particle Physics, Lund, Sweden
[81] Nagasaki Institute of Applied Science, Nagasaki, Japan
[82] Nara Women's University (NWU), Nara, Japan
[83] National and Kapodistrian University of Athens, School of Science, Department of Physics , Athens, Greece
[84] National Centre for Nuclear Research, Warsaw, Poland
[85] National Institute of Science Education and Research, Homi Bhabha National Institute, Jatni, India
[86] National Nuclear Research Center, Baku, Azerbaijan
[87] National Research Centre Kurchatov Institute, Moscow, Russia
[88] Niels Bohr Institute, University of Copenhagen, Copenhagen, Denmark
[89] Nikhef, National institute for subatomic physics, Amsterdam, Netherlands
[90] NRC Kurchatov Institute IHEP, Protvino, Russia
[91] NRNU Moscow Engineering Physics Institute, Moscow, Russia
[92] Nuclear Physics Group, STFC Daresbury Laboratory, Daresbury, United Kingdom
[93] Nuclear Physics Institute of the Czech Academy of Sciences, Řež u Prahy, Czech Republic
[94] Oak Ridge National Laboratory, Oak Ridge, Tennessee, United States
[95] Ohio State University, Columbus, Ohio, United States
[96] Petersburg Nuclear Physics Institute, Gatchina, Russia
[97] Physics department, Faculty of science, University of Zagreb, Zagreb, Croatia
[98] Physics Department, Panjab University, Chandigarh, India
[99] Physics Department, University of Jammu, Jammu, India
[100] Physics Department, University of Rajasthan, Jaipur, India
[101] Physikalisches Institut, Eberhard-Karls-Universität Tübingen, Tübingen, Germany
[102] Physikalisches Institut, Ruprecht-Karls-Universität Heidelberg, Heidelberg, Germany
[103] Physik Department, Technische Universität München, Munich, Germany
[104] Research Division and ExtreMe Matter Institute EMMI, GSI Helmholtzzentrum für Schwerionenforschung GmbH, Darmstadt, Germany
[105] Rudjer Bošković Institute, Zagreb, Croatia
[106] Russian Federal Nuclear Center (VNIIEF), Sarov, Russia
[107] Saha Institute of Nuclear Physics, Homi Bhabha National Institute, Kolkata, India
[108] School of Physics and Astronomy, University of Birmingham, Birmingham, United Kingdom
[109] Sección Física, Departamento de Ciencias, Pontificia Universidad Católica del Perú, Lima, Peru

[110] Shanghai Institute of Applied Physics, Shanghai, China

[111] St. Petersburg State University, St. Petersburg, Russia

[112] Stefan Meyer Institut für Subatomare Physik (SMI), Vienna, Austria

[113] SUBATECH, IMT Atlantique, Université de Nantes, CNRS-IN2P3, Nantes, France

[114] Suranaree University of Technology, Nakhon Ratchasima, Thailand

[115] Technical University of Košice, Košice, Slovakia

[116] Technische Universität München, Excellence Cluster 'Universe', Munich, Germany

[117] The Henryk Niewodniczanski Institute of Nuclear Physics, Polish Academy of Sciences, Cracow, Poland

[118] The University of Texas at Austin, Austin, Texas, United States

[119] Universidad Autónoma de Sinaloa, Culiacán, Mexico

[120] Universidade de São Paulo (USP), São Paulo, Brazil

[121] Universidade Estadual de Campinas (UNICAMP), Campinas, Brazil

[122] Universidade Federal do ABC, Santo Andre, Brazil

[123] University College of Southeast Norway, Tonsberg, Norway

[124] University of Cape Town, Cape Town, South Africa

[125] University of Houston, Houston, Texas, United States

[126] University of Jyväskylä, Jyväskylä, Finland

[127] University of Liverpool, Liverpool, United Kingdom

[128] University of Tennessee, Knoxville, Tennessee, United States

[129] University of the Witwatersrand, Johannesburg, South Africa

[130] University of Tokyo, Tokyo, Japan

[131] University of Tsukuba, Tsukuba, Japan

[132] Université Clermont Auvergne, CNRS/IN2P3, LPC, Clermont-Ferrand, France

[133] Université de Lyon, Université Lyon 1, CNRS/IN2P3, IPN-Lyon, Villeurbanne, Lyon, France

[134] Université de Strasbourg, CNRS, IPHC UMR 7178, F-67000 Strasbourg, France, Strasbourg, France

[135] Université Paris-Saclay Centre dÉtudes de Saclay (CEA), IRFU, Department de Physique Nucléaire (DPhN), Saclay, France

[136] Università degli Studi di Foggia, Foggia, Italy

[137] Università degli Studi di Pavia and Sezione INFN, Pavia, Italy

[138] Università di Brescia and Sezione INFN, Brescia, Italy

[139] Variable Energy Cyclotron Centre, Homi Bhabha National Institute, Kolkata, India

[140] Warsaw University of Technology, Warsaw, Poland

[141] Wayne State University, Detroit, Michigan, United States

[142] Westfälische Wilhelms-Universität Münster, Institut für Kernphysik, Münster, Germany

[143] Wigner Research Centre for Physics, Hungarian Academy of Sciences, Budapest, Hungary

[144] Yale University, New Haven, Connecticut, United States

[145] Yonsei University, Seoul, Republic of Korea